

# Dynamic analysis of a functionally graded tapered rotating shaft under thermal load via differential quadrature finite elements method

Fethi Hadjoui<sup>1a</sup>, Ahmed Saimi<sup>\*1,2</sup>, Ismail Bensaid<sup>1a</sup> and Abdelhamid Hadjoui<sup>1b</sup>

<sup>1</sup>IS2M Laboratory, Faculty of Technology, University of Tlemcen, Algeria

<sup>2</sup>National Higher School of Hydraulic, Blida, Algeria

(Received April 26, 2022, Revised December 23, 2022, Accepted January 6, 2023)

**Abstract.** The present study proposes a theoretical and numerical investigation on the dynamic response behaviour of a functional graded (FG) ceramic-metal tapered rotor shaft system, by the differential quadrature finite elements method (DQFEM) to identify the natural frequencies for modelling and analysis of the structure with suitable validations. The purpose of this paper is to explore the influence of heat gradients on the natural frequency of rotation of FG shafts via three-dimensional solid elements, as well as a theoretical examination using the Timoshenko beam mode, which took into account the gyroscopic effect and rotational inertia. The functionally graded material's distribution is described by two distribution laws: the power law and the exponential law. To simulate varied thermal conditions, radial temperature distributions are obtained using the nonlinear temperature distribution (NLTD) and exponential temperature distribution (ETD) approaches. This work deals with the results of the effect on the fundamental frequencies of different material's laws gradation and temperature gradients distributions. Attempts are conducted to identify adequate explanations for the behaviours based on material characteristics. The effect of taper angle and material distribution on the dynamic behaviour of the FG conical rotor system is discussed.

**Keywords:** DQFEM; exponential temperature distribution; functionally graded material; non-linear temperature distribution; rotor dynamics; tapered shaft

## 1. Introduction

Scientific research has grown in recent years employing ceramic materials to suit the expanding needs of the mechanical engineering sector under the effect of temperatures, with these new materials having a good feature of resistance to high temperatures. However, due to their low hardness, ceramics alone have limited applications in the mechanical industry. FG materials are a novel type of composite material that has recently piqued the interest of scientific and industrial researchers. These materials are non-homogeneous, comprising of multiple layers of progressive mixes of components, most of which are ceramic and metal. Ceramic constituents can endure high temperatures because of their thermal barrier qualities, whereas metal supports the performance of

---

\*Corresponding author, Ph.D., E-mail: ahmedsaimi@hotmail.fr

<sup>a</sup>Ph.D.

<sup>b</sup>Professor

the strongest mechanical capabilities in FG materials. A group of Japanese scientists coined the term FGM in the mid-1980s. (Yamanouchi *et al.* 1990). Since then, a lot of work has gone into developing these materials, which are extremely resistant to temperature changes. (Hirai and Chen 1999a, Hirai and Chen 1999b, Uemura 2003) FG materials were originally proposed as a lightweight, high temperature refractory material for aerospace constructions, fusion reactors, and engines. The concept of FGM, mathematical modelling, fabrication methods, material evaluation, applications, joining procedures in FGM, process characterization, and design considerations are all covered in (Holt *et al.* 1993). (Reddy and Chin 1998) studied the dynamic thermoelastic response of functionally graded cylinders and plates by varying the volume fraction of a ceramic and a metal using a power law distribution, including the thermomechanical coupling, and a finite element model. FG materials are currently being developed for more widespread applications as high-performance structural components. As a result, scientific study on this axis and its industrial use has continued, with the fabrication of gas turbine blades constructed of FG materials (Librescu *et al.* 2005). The production of rotors made of FG materials for aircraft reactors and propulsion turbines for aeronautics has increased the use of these materials. Scientific research, in particular that of (Przybyłowicz 2005), has advanced this development by studying the stability of a rotor composed of FG materials, as well as the active stabilization of a rotating FG shaft with a piezoelectric fraction to manage thermal stresses. (Cheng *et al.* 2006) used the assumed mode approach with coupling effect to investigate the frequency analysis of a spinning cantilever beam. (Boukhalfa and Hadjoui 2010) used the h-p version of the finite element method to investigate the free vibrations of an on-board rotor built of composite materials. (Saimi and Hadjoui 2016) used the h-p variant of the finite element method to model an on-board rotor. (Akbaş 2014) investigated the vibrational behaviour of a beam formed of FG materials in a temperature-varying environment. (Boukhalfa 2014) used the -p variant of the finite element method to investigate the dynamic behavior of a rotor composed of FG materials. (Ding *et al.* 2018) investigated the nonlinear vibration response of functionally graded (FG) Euler–Bernoulli beams on elastic foundation, taking into account the effects of the cross-section rotary inertia and neutral surface position. (Rao and Roy 2016) used the finite element method version -h to do a dynamic study of an FG rotor, and they used the power law method to describe the FG rotor based on Timoshenko's theory. (Bouzidi *et al.* 2021) conducted a comparative study between the functionally graded and pure metallic rotor-blade systems using the h- version of the finite element method, and the comparison was based on the influence of the blade's numbers, rotating speed, and power law index on the natural frequencies of the rotor-blade system. (Gayen *et al.* 2017b) investigated the dynamic behavior of a functionally graded shaft with a transvers crack using two noded Timoshenko beam elements and a finite element formulation. In the same research axis, (Gayen *et al.* 2017a) looked at the impact of multiple breathing cracks on a functionally graded rotating Thy have also studied the stability analysis of a rotor-bearing system having a functionally graded shaft with transverse breathing cracks, with finite element method (Gayen *et al.* 2019). A Numerical analysis on the dynamic's behaviour of symmetrical FGM rotor in thermal environment using h-p finite element method was also studied by (Assem *et al.* 2022). (Bose and Sathujoda 2020) studied the effect of Thermal Gradient on Vibration Characteristics of a Functionally Graded symmetrical rotor shaft using classic finite element modelling with ANSYS. Recently (Gayen *et al.* 2021) also studied the dynamic behaviour of two-cracked functionally graded (FG) shaft system under thermal environment; a formulation based on finite elements was used to model metal-ceramic FG (SS/ZrO<sub>2</sub>) shaft using Timoshenko beam theory, with power law distribution of the material gradation, with a conclusion that the local flexibility coefficients are functions of material gradient

and temperature besides crack size. Even though the reduction in Eigen frequencies is decided by crack parameters, material gradient and temperature, however, the reduction in Eigen frequencies is greatly influenced by gradient index and the index may be selected properly to design FG shafts for high-temperature applications. A newly modelling method DQFEM was applied for the modelling of rotor dynamics in the paper (Ahmed *et al.* 2020). The developed methods and applications have shown clearly that convergence was obtained for a low sampling and item numbers when compared with h-FEM and hp-FEM. The DQFEM was firstly used by (Xing and Liu 2009) for studying the high-accuracy differential quadrature finite element method and its application to free vibrations of thin plate with curvilinear domain. (Zahi *et al.* 2018) presented a theoretical and numerical analysis of the behaviour of a tapered shaft rotor built of composite materials using the finite element method's classical version h and version p. (Torabi *et al.* 2017) examined the exact solution for two-plane transverse vibration analysis of axial-loaded multi-step Timoshenko rotor carrying concentrated masses is presented. (Torabi *et al.* 2014) used the DQEM for free transverse vibration analysis of multiple cracked non-uniform Timoshenko beams with general boundary conditions. (Pouretamad *et al.* 2019b) employed a differential quadrature element method (DQEM) is proposed for free vibration analysis of rotating non-uniform nanocantilevers carrying multiple concentrated masses. (Pouretamad *et al.* 2019a) investigated the free transverse vibration characteristics of a rotating non-uniform nanocantilever with multiple open cracks. (Afshari and Irani Rahaghi 2018) analysed the free transverse vibration of multi-stepped rotors resting on multiple bearings via the differential quadrature element method. (Afshari *et al.* 2022) presented an exact solution for whirling analysis of rotors carrying concentrated masses. Effect of various parameters on the forward and backward frequencies are investigated including velocity of spin and quantity, translational inertia and position of the concentrated masses

Following the preceding literatures, this work investigates the dynamic behaviour of a functionally graded tapered hollowed shaft in a thermal environment using a combined method involving the differential quadrature method and the classical finite element method, dubbed the DQFEM (Ahmed *et al.* 2020). The Lagrange's equation and the Timoshenko beam theory are used to obtain the global equation of motion. The shaft is made of functionally graded (FG) materials. Using the power law and the exponential law as deferent approaches. The system's natural frequencies are determined using a MATLAB tool, and the results are compared to those described in the literature. A study that compares the effects of exponential and NLTD. The frequencies are measured to assess the effect of the tapered angle on the shaft's vibration resistance as a function of temperature. The results suggest that functionally graded materials are more efficient and appropriate for shaft modelling, design, and conceptualization.

## 2. Functionally graded Material and temperature distribution laws

The exact gradation shapes of the FG material are not available. However, there are different mathematical laws that can be used to represent the distribution of the volume fraction in the FG material.

The properties of the material vary according to the volume fraction distribution as shown in Fig. 1 (Aboudi *et al.* 1999) which shows the continuously graded microstructure of an FG material. In the case of FG shaft, the volume fraction varies in the radial direction (Gayen and Roy 2014) as shown in Fig. 2. The first inner layer of the shaft is composed purely of metal, as one

moves towards the radial outer direction the fractional volume of the metal decreases, and that of the ceramic increases. Thus, the outer layer is 100 per cent ceramic, which gives excellent temperature resistance properties. The position dependence is obtained using the Voigt model, which gives a simple rule for composite materials. The material properties for each layer are expressed in Eq. (1).

$$P_i = P_c V_c + P_m V_m \quad (1)$$

Where  $P_c$  and  $P_m$  are the material properties of the ceramic and metal, respectively, and  $V_c$  and  $V_m$  refer to the volume fraction of the ceramic and metal, respectively. Different mathematical models have been developed over the years by researchers to accurately predict the distribution. These include the power law, the exponential law, the sigmoid law and the Mori-Tanka scheme, which are the most widely, used laws for the gradation of FG materials. However, the majority of previous works have used the gradation of the power law in the case of FG shafts. In this present work, power law, gradation and exponential law gradation have been applied to tapered shaft rotor systems. Modelling using these laws and their application have been discussed in detail in the subsections.

The main purpose of FG materials is temperature resistance. The properties of FG materials depend on the variation in temperature. In most cases of FG shafts, the outer ceramic material is subjected to higher temperatures than the inner metal core. This difference in gradation generates a radial variation of the material properties in the shaft. The temperature dependent properties have been proposed by (Touloukian 1966) as in the Eq. (2).

where  $P_0, P_{-1}, P_1, P_2$  and  $P_3$  indicate the coefficients of temperature  $T$  (in Kelvin) for each type of material that makes up the volume proportion of FG materials' gradation (Reddy and Chin 1998).

$$P_j = P_0(P_{-1}T^{-1} + 1 + P_1T^1 + P_2T^2 + P_3T^3) \quad (2)$$

Various combinations of FG materials were used in this work. Hence, the inner metallic material is SUS304 stainless steel, and the outer ceramic materials are Nickel,  $Al_2O_3$ , Zr

Table 1 Temperature coefficients

Materials	Property	$P_{-1}$	$P_0$	$P_1$	$P_2$	$P_3$
SUS304	$E$ (Pa)	0	$201.04 \times 10^9$	$3.079 \times 10^{-4}$	$-6.534 \times 10^{-7}$	0
	$K$ (W/mK)	0	15.379	$-1.264 \times 10^{-3}$	$2.092 \times 10^{-6}$	$-7.223 \times 10^{-10}$
	$\nu$	0	0.3262	$-2.002 \times 10^{-4}$	$3.797 \times 10^{-7}$	0
Nickel	$E$ (Pa)	0	$223.95 \times 10^9$	$-2.794 \times 10^{-4}$	$-3.998 \times 10^{-9}$	0
	$K$ (W/mK)	0	58.754	$-4.614 \times 10^{-4}$	$6.670 \times 10^{-7}$	$-1.523 \times 10^{-10}$
	$\nu$	0	0.3100	0	0	0
$Al_2O_3$	$E$ (Pa)	0	$349.5486 \times 10^9$	$-3.853206 \times 10^{-4}$	$4.026993 \times 10^{-7}$	$-1.6734 \times 10^{-10}$
	$K$ (W/mK)	-1123.6	-14.087	0.00044	0	0
	$\nu$	0	0.26	0	0	0
Zr	$E$ (Pa)	0	$244.27 \times 10^9$	$-1.371 \times 10^{-3}$	$1.214 \times 10^{-6}$	$-3.681 \times 10^{-10}$
	$K$ (W/mK)	0	1.7000	$1.276 \times 10^{-4}$	$6.648 \times 10^{-8}$	0
	$\nu$	0	0.2882	$1.133 \times 10^{-4}$	0	0
Silicon Nitride	$E$ (Pa)	0	$348.43 \times 10^9$	$-3.070 \times 10^{-4}$	$2.160 \times 10^{-7}$	$-8.946 \times 10^{-11}$
	$K$ (W/mK)	0	13.723	$-1.032 \times 10^{-3}$	$5.466 \times 10^{-7}$	$-7.876 \times 10^{-11}$
	$\nu$	0	0.244	0	0	0

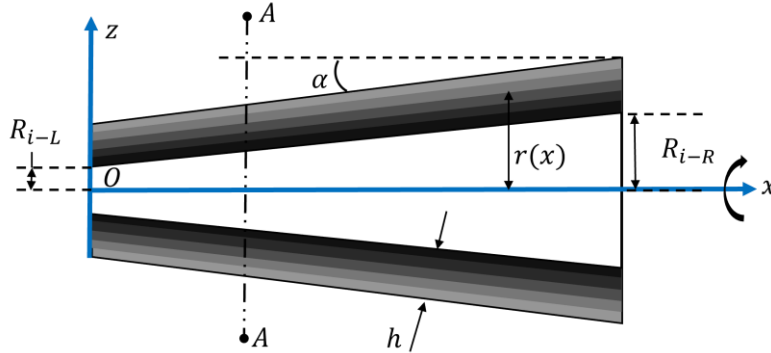


Fig. 1 Modelling of the FGM tapered rotor shaft

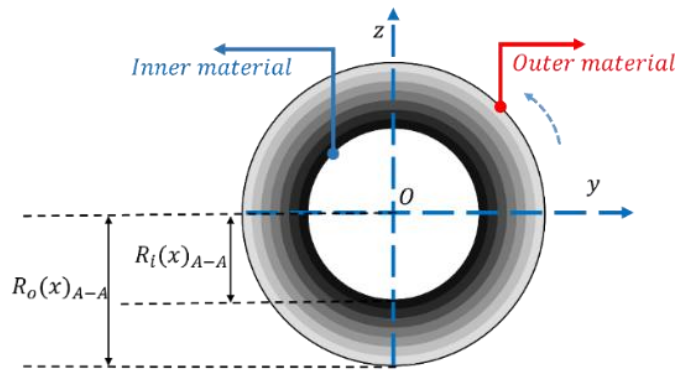


Fig. 2 Section cut A-A from Fig. 1

(Zircon), Silicon Nitride. The temperature coefficients can be obtained from the works of (Reddy and Chin 1998). These coefficients are shown in Table 1.

The responses of the thermomechanical behaviour of FG materials can be accurately modelled using different temperature distribution methods, such as ETD and non-linear temperature distribution. The properties of materials that are influenced by temperature are Young's modulus, Poisson's coefficient, and thermal conductivity, while density does not change with temperature.

The geometric parameters  $R_{i-L}$ ,  $R_{i-R}$ ,  $R_o(x)$ ,  $R_i(x)$  indicated in Figs. 1 and 2, are: the left inner radius, right inner radius, outer radius, and inner radius respectively.

With  $D_L = 2 * R_{i-L}$  left internal diameter.

Responses to the thermomechanical effects of FG materials can be modelled using different temperature distribution methods, which can be found in the literature.

In the case of a symmetrical solid cylinder, assuming that there is no heat generation and numerically solving the differential thermal conduction equation with appropriate boundary conditions, as shown in the equation (3) gives the radial temperature distribution profiles.

$$\frac{d}{dr} \left( rK(r, T) \frac{dT}{dr} \right) = 0 \quad (3)$$

### 2.1 Exponential law gradation with ETD

Few researchers have used the exponential law on FG tapered shafts. The position-dependent properties of the FG material using the exponential law for a tapered FG shaft of circular cross-section can be given as (Afsar and Go 2010) shown in the Eq. (4).

Considering a tapered elastic shaft of circular cross section, the  $x$  and  $y$  coordinates define the horizontal plane of the shaft, while the  $z$ -axis defines the vertical plane with the other axes, Fig. 2.

$$P(r(x)) = P_m \exp(\lambda(x)(r(x) - R_i(x))) \quad , x \in [0, L] \quad (4)$$

$$\text{with } \lambda(x) = \frac{1}{(R_o(x) - R_i(x))} \ln\left(\frac{P_c}{P_m}\right) \quad (5)$$

$P(r(x))$  refers to the position-dependent properties of the material  $r(x)$ .  $P_c$  and  $P_m$  are properties of the ceramic- and metal-rich region, respectively. This law governs all material properties obtained from the literature.

Where  $r(x)$  denotes the variation of the radius  $r$  as a function of position  $x$ , depending on the conicity of the hollow rotor system. The inner surface of the shaft ( $r(x) = R_i(x)$ ) consists of 100% material ( $i$ ), while the outer surface of the shaft ( $r(x) = R_o(x)$ ) has 100% material ( $o$ ). ETD could be obtained using the thermal conductivity following the exponential variation for the circular cross section beams/shafts or cylinders as showed in Eqs. (6)-(9) (Gayen *et al.* 2019).

$$T(r(x)) = A(x) + B(x) \exp^{-(\beta(x)(r(x) - R_i(x)))} \quad (6)$$

With

$$A(x) = T_m - \frac{(T_c - T_m)}{\exp^{-(\beta(x)(R_o(x) - R_i(x)))} - 1} \quad (7)$$

$$B(x) = \frac{(T_c - T_m)}{\exp^{-(\beta(x)(R_o(x) - R_i(x)))} - 1} \quad (8)$$

$$\text{with } \beta(x) = \frac{1}{(R_o(x) - R_i(x))} \ln\left(\frac{K_c}{K_m}\right) \quad (9)$$

$T(r(x))$  is the temperature at the radial distance " $r(x)$ ".  $T_c$  and  $T_m$  are temperatures in ceramic-rich and metal-rich regions, respectively. Position-dependent material properties in ceramic-rich and metal-rich regions are denoted by  $P_m$  and  $P_c$ , respectively. The temperature distribution law is denoted by Eq. (6), and it can be used for FG shaft analysis where exponential gradation is desired.

Fig. 3 shows the exponential temperature variation in the radial direction of a hollow FG shaft when the temperature varies from 300K to 900K from the inside to the outside, hence the geometrical properties of the shaft taken are: ( $h = 0.002$  m;  $D_L = h * 500$ ;  $L = D_L * 20$ ).

Fig. 4 shows the Young's modulus variation when the temperature is constant (300K), and also when the temperature varies from 300K to 900K from the inside to the outside. Fig. 5 shows that temperature has no influence on density. According to Figs. 3-5, the properties of FG materials have an exponential rate regardless of geometry.

## 2.2 Power law gradation with non-linear temperature distribution

The power law is the most widely utilized law to determine FG material gradation. It is a well-

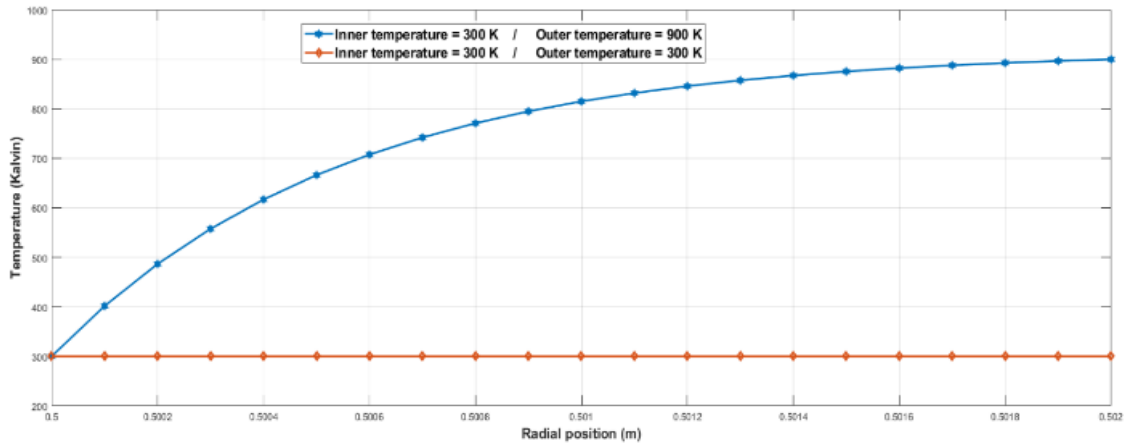


Fig. 3 Temperature distribution profile using ETD in SS-Al<sub>2</sub>O<sub>3</sub> FG hollowed shaft

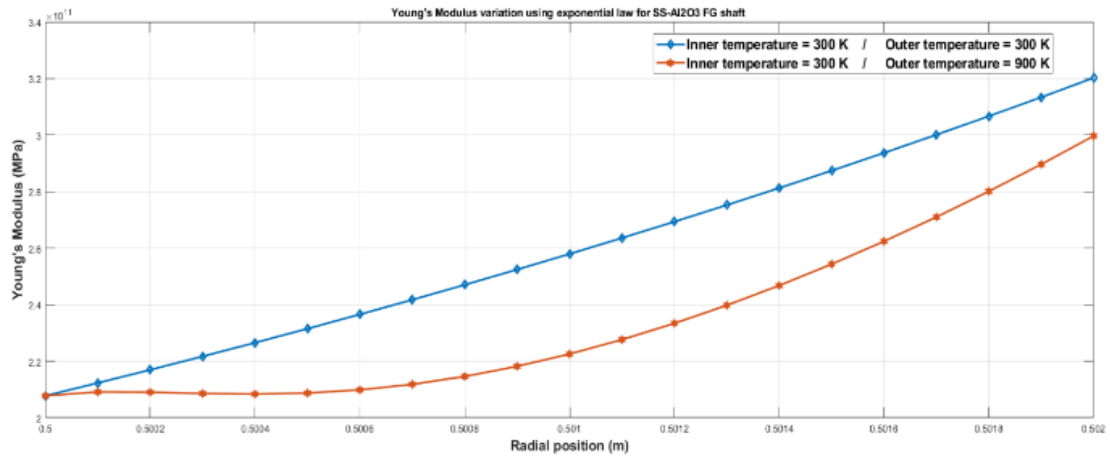


Fig. 4 Young's Modulus variation using exponential law for SS-Al<sub>2</sub>O<sub>3</sub> FG hollowed shaft

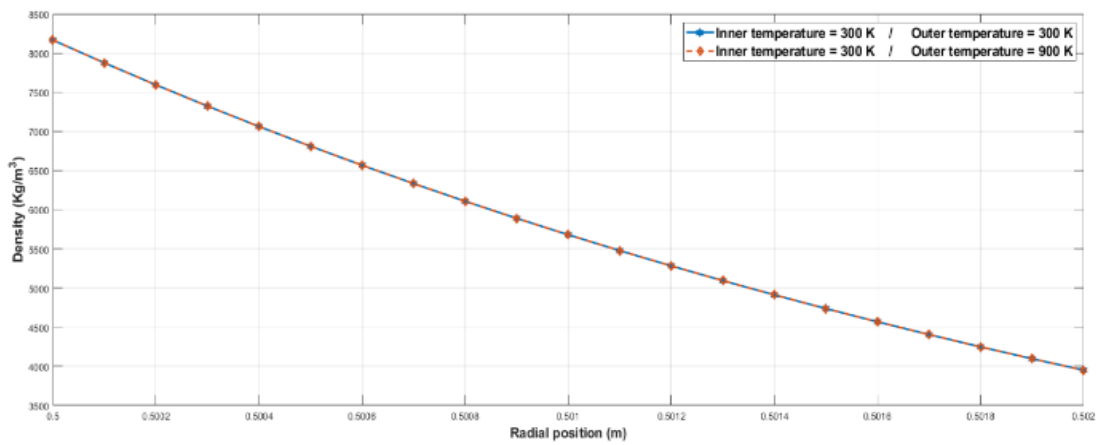


Fig. 5 Density variation using exponential law for SS-Al<sub>2</sub>O<sub>3</sub> FG hollowed shaft

known model that has been widely used to simulate the behaviour of FG plates, shafts, and other components. (Reddy and Chin 2007) using Eq. (10)

$$P(r(x)) = [P_c - P_m] \left( \frac{r(x) - R_i(x)}{R_o(x) - R_i(x)} \right)^k + P_m \quad (10)$$

$P(r(x))$  denotes radially varying material properties like Young's modulus, Poisson's ratio, thermal conductivity (K), density, and coefficient of thermal expansion.

In the ceramic-rich and metal-rich regions,  $P_m$  and  $P_c$  are temperature-dependent material properties. These are obtained by solving differential Eq. (3) at the metal and ceramic temperatures, respectively.  $R_o$  and  $R_i$  are the cylinder's outer and inner radius, respectively. The power law index is denoted by "k".  $V_o(r(x)) = \left( \frac{r(x) - R_i(x)}{R_o(x) - R_i(x)} \right)^k$  denotes the volume fraction of metal at a median radius ' $r(x)$ ' of any layer.

The non-linear temperature distribution has been researched in FG materials research and is employed with power law gradation. This is the solution to Eq. (3) when the boundary conditions are met and the first seven terms of the polynomial expansion are taken into account (Kiani and Eslami 2010). gives the Eq. (11)

$$T(r(x)) = T_m + (T_c + T_m)\Gamma(x) \quad (11)$$

With

$$\Gamma(x) = \frac{\left[ \sum_{j=0}^5 \left( \frac{(-1)^j}{jk+1} \left( \frac{K_{cm}}{K_m} \right)^j \left( \frac{r(x) - R_i(x)}{R_o(x) - R_i(x)} \right)^{jk+1} \right) \right]}{\left[ \sum_{j=0}^5 \left( \frac{(-1)^j}{jk+1} \left( \frac{K_{cm}}{K_m} \right)^j \right) \right]} \quad (12)$$

Where,  $K_{cm} = K_c - K_m$ .  $K_c$  and  $K_m$  refer to the thermal conductivity of regions rich in ceramics and metals at a given temperature.  $K_c$  and  $K_m$  depend on the temperature and are also calculated using the Eq. (2) at respective metal and ceramic temperatures.

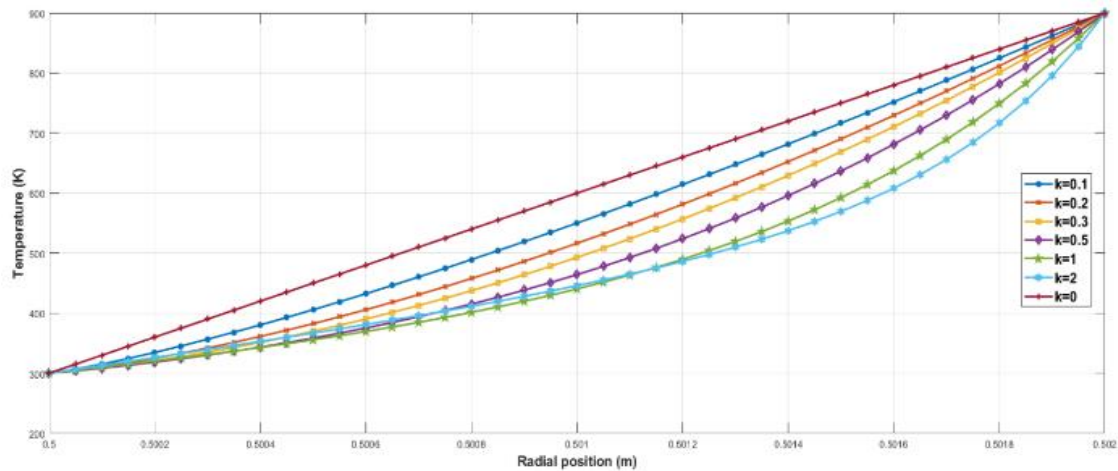


Fig. 6 Temperature distribution profile using NLTD in SS-Al<sub>2</sub>O<sub>3</sub> FG hollowed shaft

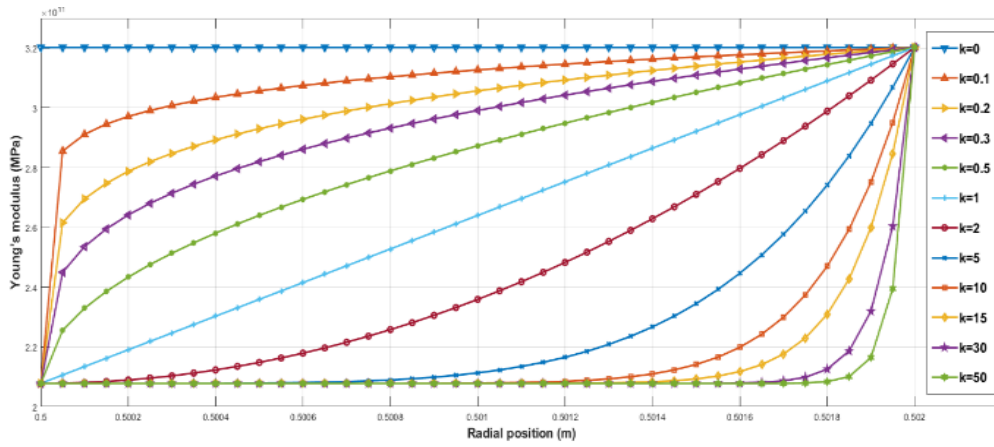


Fig. 7 Variation of FG materials' Young's modulus as a function of the fractional volume index  $k$  in the radial direction (300K-300K) SS-Al<sub>2</sub>O<sub>3</sub> FG shaft

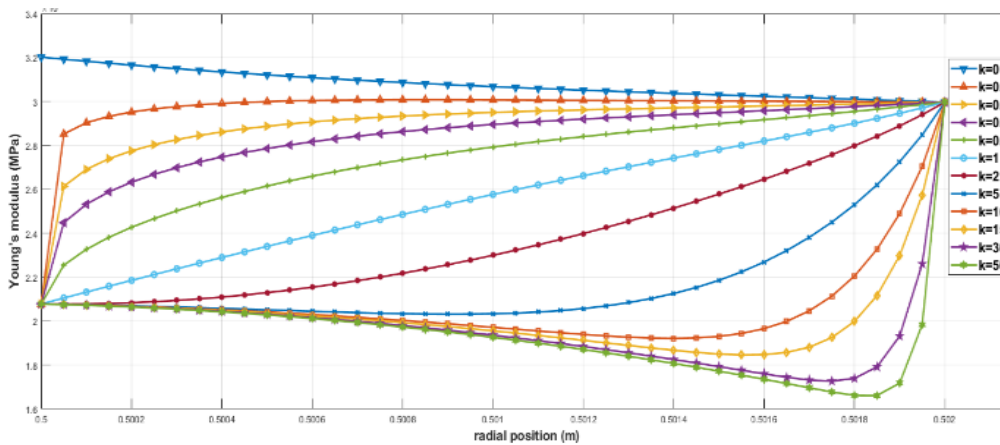


Fig. 8 Variation of FG materials' Young's modulus as a function of the fractional volume index  $k$  in the radial direction (300K-900K) SS-Al<sub>2</sub>O<sub>3</sub> FG shaft

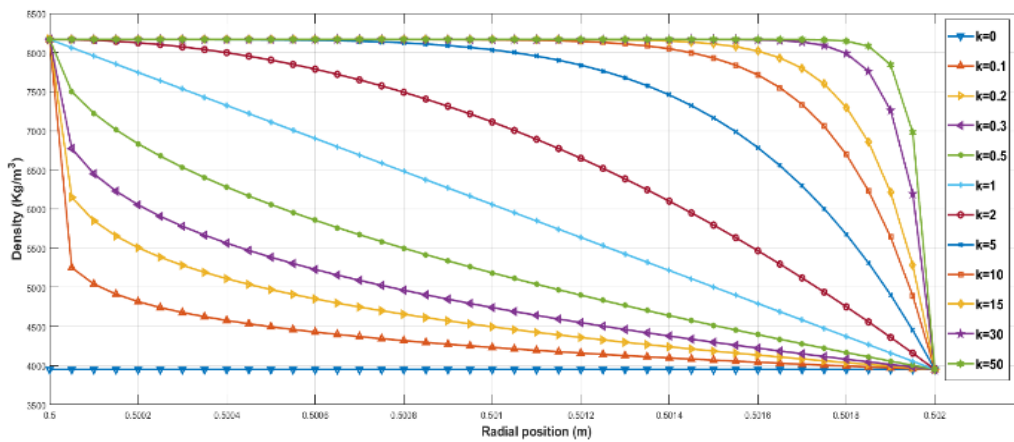


Fig. 9 Variation of FG material density as a function of fractional volume index  $k$  in the radial direction

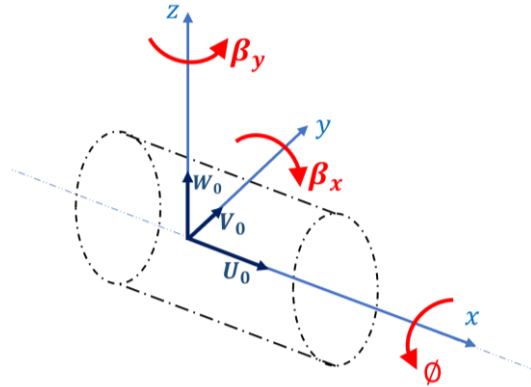


Fig. 10 Displacements in 3 dimensions

Figs. 7-9 show the variations in temperature, Young's modulus and density respectively for the volume fraction index.

The variation in the properties of FG materials can be seen in the curves in Figs. 6-9 which show the variation in temperature, Young's modulus, and density of a geometric FG shaft ( $h = 0.002$  m;  $D_L = h * 500$ ;  $L = D_L * 20$ ). According to the power law, these properties are a function of the gradation index of the volume fraction, which can vary in the radial direction of the shaft.

$k=0$  means that the shaft is made of pure ceramic,

$k=\infty$  means that the shaft is made of pure metal

$k=1$  indicates linear gradation.

The temperature distribution in the FG layer is nonlinear, as illustrated in Fig. 6. This is because thermal conductivity, modulus of elasticity, and density are all functions of shaft radius alone. The temperature distribution is a straight line for  $k=0$  and  $k=1$  and is independent of the shaft's material properties. The temperature distribution depends on radial positions, material properties, and the law of gradation for other values of  $k$ , as shown in Table 1. According to Table 1, the temperature gradually increases from  $k=0$  to a certain value of the power law index, then begins to decrease until it reaches the initial value in value  $k=\infty$ .

### 3. Formulation of a motion equation.

The rotor model shown in Fig. 10 is investigated in this work. The following kinematic hypotheses in Timoshenko's model: the displacement fields ( $U, V, W$ ) showed in Fig. 10 at any position in the cross section of the shaft are provided by the relation (13) (Irani Rahagi *et al.* 2016).

$$\begin{cases} U(x, y, z, t) = U_0(x, t) + z\beta_x(x, t) - y\beta_y(x, t) \\ V(x, y, z, t) = V_0(x, t) - z\phi(x, t) \\ W(x, y, z, t) = W_0(x, t) + y\phi(x, t) \end{cases} \quad (13)$$

$U, V, W$  indicating the bending displacements of any point on the shaft along the x-axis, y-axis, and z-axis respectively.

$U_0, V_0$  and  $W_0$ , indicating the initial displacements of the bending of any point on the shaft.

$\beta_x$  and  $\beta_y$ , representing the rotational angles with respect to the  $y$  and  $z$  axes.

$z\beta_x$ : is the displacement caused by the rotation of the shaft's cross section caused by bending and shears along the  $z$  axis.

$y\beta_y$ : is the displacement due to the rotation of the cross section of the shaft induced by bending and shears along the  $y$  axis.

$z\phi(x, t)$ : is the displacement caused by the  $z$ -axis twist's rotation of the cross section.

$y\phi(x, t)$ : displacement caused by cross-sectional rotation due to torsion along the  $y$  axis.

$\phi(x, t)$ : cross section rotation around the  $x$  axis.

### 3.1 Strain energy

Cylindrical coordinate system deformations  $(x, r, \theta)$  (MinYung *et al.* 2004)

$$\begin{cases} \varepsilon_{xx} = \frac{\partial U_0}{\partial x} + r \sin\theta \frac{\partial \beta_x}{\partial x} - r \cos\theta \frac{\partial \beta_y}{\partial x} \\ \varepsilon_{x\theta} = \frac{1}{2} \left( \beta_y \sin\theta + \beta_x \cos\theta - \sin\theta \frac{\partial V_0}{\partial x} + \cos\theta \frac{\partial W_0}{\partial x} \right) + r \frac{\partial \phi}{\partial x} \\ \varepsilon_{xr} = \frac{1}{2} \left( \beta_x \sin\theta - \beta_y \cos\theta - \sin\theta \frac{\partial W_0}{\partial x} + \cos\theta \frac{\partial V_0}{\partial x} \right) \end{cases} \quad (14)$$

The stress strain relation in cylindrical coordinates  $(x, r, \theta)$  in the matrix form can be written (Berthelot 1996)

$$\begin{bmatrix} \sigma_{xx} \\ \tau_{x\theta} \\ \tau_{xr} \end{bmatrix} = \begin{bmatrix} C'_{11} & 0 & k_s C'_{16} \\ k_s C'_{16} & 0 & k_s C'_{66} \\ 0 & k_s C'_{55} & 0 \end{bmatrix} \begin{bmatrix} \varepsilon_{xx} \\ \gamma_{x\theta} \\ \gamma_{xr} \end{bmatrix} \quad (15)$$

$k_s$ : is the shear correction factor.

$C'_{ij}$  Constants of elasticity compared to the principal axes.

The strain energy of FG shaft materials is expressed by replacing the Eqs. (14) and (15) in Eq. (16) to get Eq. (17).

$$E_{da} = \frac{1}{2} \int (\sigma_{xx} \varepsilon_{xx} + 2\tau_{xr} \gamma_{xr} + 2\tau_{x\theta} \gamma_{x\theta}) dV \quad (16)$$

$$\begin{aligned} E_{da} = & \frac{1}{2} \int_0^L A_{11}(x) \left( \frac{\partial U_0}{\partial x} \right)^2 dx + \frac{1}{2} \left[ \int_0^L B_{11}(x) \left( \frac{\partial \beta_x}{\partial x} \right)^2 dx + \int_0^L B_{11}(x) \left( \frac{\partial \beta_y}{\partial x} \right)^2 dx \right] + \\ & \frac{1}{2} k_s \int_0^L B_{66}(x) \left( \frac{\partial \phi}{\partial x} \right)^2 dx + \frac{1}{2} k_s \left[ \int_0^L (A_{55}(x) + A_{66}(x)) \left( \frac{\partial V_0}{\partial x} \right)^2 dx + \int_0^L (A_{55}(x) + \right. \\ & A_{66}(x)) \left( \frac{\partial W_0}{\partial x} \right)^2 dx + \int_0^L (A_{55}(x) + A_{66}(x)) \beta_x^2 dx + \int_0^L (A_{55}(x) + A_{66}(x)) \beta_y^2 dx + \\ & \left. 2 \int_0^L (A_{55}(x) + A_{66}(x)) \beta_x \frac{\partial W_0}{\partial x} dx - 2 \int_0^L (A_{55}(x) + A_{66}(x)) \beta_y \frac{\partial V_0}{\partial x} dx \right] \end{aligned} \quad (17)$$

The terms  $A_{11}, A_{55}, A_{66}, B_{11}$  of the Eqs. (18)-(24) given as follows

$$A_{11}(x) = 2\pi \int_{R_i(x)}^{R_o(x)} Q_{11}(r) r dr \quad (18)$$

$$A_{55}(x) = \pi \int_{R_i(x)}^{R_o(x)} Q_{55}(r) r dr \quad (19)$$

$$A_{66}(x) = \pi \int_{R_i(x)}^{R_o(x)} Q_{66}(r) r dr \quad (20)$$

$$B_{11}(x) = \pi \int_{R_i(x)}^{R_o(x)} Q_{11}(r) r^3 dr \quad (21)$$

$$B_{66}(x) = \pi \int_{R_i(x)}^{R_o(x)} Q_{66}(r) r^3 dr \quad (22)$$

$$Q_{11}(r) = \frac{E(r)}{1-\vartheta(r)^2} \quad (23)$$

$$Q_{55}(r) = Q_{66}(r) = \frac{E(r)}{2(1+\vartheta(r))} \quad (24)$$

### 3.2 Kinetic energy of the shaft

The rotor studied at an angular velocity  $\Omega$  and a total length  $L$ , its kinetic energy is defined by: (Boukhalifa 2014)

$$E_{ca} = \frac{1}{2} \int_0^L \left( I_m(x) (\dot{U}_0^2 + \dot{V}_0^2 + \dot{W}_0^2) + I_d(x) (\dot{\beta}_x^2 + \dot{\beta}_y^2) - 2\Omega I_p(x) \beta_x \dot{\beta}_y^2 + \Omega^2 I_d(x) (\beta_x^2 + \beta_y^2) + \Omega^2 I_p(x) \right) dx \quad (25)$$

The term  $2\Omega I_p(x) \beta_x \dot{\beta}_y^2$  represents the gyroscopic effect and the term  $I_d(x) (\dot{\beta}_x^2 + \dot{\beta}_y^2)$  represents the rotational inertia effect.

$I_m(x)$ : Mass moment of inertia.

$I_d(x)$ : diametric moment of inertia

$I_p(x)$ : polar moment of inertia of the shaft per unit of length.

The term  $\Omega^2 I_d(x) (\beta_x^2 + \beta_y^2)$  representing the centrifugal stiffening, which is very small, in front of  $\Omega^2 I_p(x)$  which will be neglected later.

$$I_m(x) = 2\pi \int_{R_i(x)}^{R_o(x)} \rho(r) r dr \quad (26)$$

$$I_d(x) = \pi \int_{R_i(x)}^{R_o(x)} \rho(r) r^3 dr \quad (27)$$

$$I_p(x) = 2\pi \int_{R_i(x)}^{R_o(x)} \rho(r) r^3 dr \quad (28)$$

With

$$\begin{cases} R_i(x) = \tan(\alpha) x + R_{i-L} \\ R_o(x) = \tan(\alpha) x + (R_{i-L} + h) \end{cases} \quad (29)$$

$$\tan(\alpha) = \frac{R_{i-R} - R_{i-L}}{L} \quad (30)$$

$R_{i-L}$ : Tapered shaft left inner radius.

$R_{i-R}$ : Tapered shaft Right inner radius.

#### 4. Modelling by the deferential quadrature finite elements method.

The deferential quadrature finite elements method was used to solve the governing equations. The differential quadrature rules and Gauss-Lobatto quadrature are used to discretize the system energies.

In the differential quadrature rules, derivative of any order of a function is approximated by a weighted linear sum of the function values at all the discrete points. Taking a function  $f(x, t)$  as an example, the mathematic description of the GDQM is given by (Hua and Lam 1998)

Thus, for a field variable  $f(x)$  its derivative of order  $n$  in a discrete point  $x_i$  can be expressed as

$$\left. \frac{\partial^n f(x, t)}{\partial x^n} \right|_{x_i} = \sum_{j=1}^N W_{ij}^{(n)} f(x_j, t) \quad (i = 1, 2, 3, \dots, N) \quad (31)$$

With  $W_{ij}^{(n)}$  is the weighting coefficient related to the derivative of order  $n$ , and the weighting coefficient is obtained as follows

if  $n = 1$ , so

$$\begin{aligned} W_{ij}^{(1)} &= \frac{M(x_i)}{(x_i - x_j)M(x_j)} \quad i \neq j, i, j = 1, 2, \dots, N \\ W_{ii}^{(1)} &= -\sum_{j=1, j \neq i}^N W_{ij}^{(1)} \quad i = 1, 2, \dots, N \end{aligned} \quad (32)$$

where

$$\begin{aligned} M(x_i) &= \prod_{k=1, k \neq i}^N (x_i - x_k) \\ M(x_j) &= \prod_{k=1, k \neq i}^N (x_j - x_k) \end{aligned} \quad (33)$$

If  $n > 1$ , secondary and higher order derivatives, the weighting coefficients are determined using the following simple recurrence relationship:

$$\begin{aligned} W_{ij}^{(n)} &= n \left( W_{ij}^{(1)} * W_{ii}^{(n-1)} - \frac{W_{ij}^{(n-1)}}{(x_i - x_j)} \right) \quad i \neq j, i, n > 1 \\ & \quad j = 1, 2, \dots, N \\ W_{ii}^{(n)} &= -\sum_{j=1, j \neq i}^N W_{ij}^{(n)} \quad i = 1, 2, \dots, N \end{aligned} \quad (34)$$

To get denser population near boundaries, the sampling points are selected based on the Chebyshev-Gauss-Lobatto grid distribution.

$$x_j = \frac{L}{2} \left[ 1 - \cos \left( \frac{j-1}{N-1} \pi \right) \right] \quad j = 1, 2, \dots, N \quad (35)$$

The theory of Gauss-Lobatto quadrature rules can be found in the mathematical literature; The Gauss-Lobatto quadrature rule with a degree of accuracy  $(2n - 3)$  for the function  $f(x)$  defined in  $[-1, 1]$  is

$$\int_{-1}^1 f(x) dx = \sum_{j=1}^N C_j f(x_j) \quad (36)$$

With the weighting coefficient  $C_j$  of the Gauss-Lobatto, integration is given by

$$C_1 = C_N = \frac{2}{N(N-1)}, \quad C_j = \frac{2}{N(N-1)[P_{N-1}(x_j)]^2} \quad (j \neq 1, N) \quad (37)$$

$x_j$  is the  $(j - 1)$  zero of the first order derivative of  $P_{N-1}(x)$ . To solve the roots of the

Legendre polynomials, it will use the recursivity formula as Eqs. (38) and (39); it is easy to obtain thousands of roots.

$$P_{N+1}(x) = \frac{2N+1}{N+1} x P_N(x) - \frac{N}{N+1} P_{N-1}(x) \quad (38)$$

With  $P_0(x) = 1$ ,  $P_1(x) = x$ . The  $n$ th-order derivation of the Legendre polynomials can be determined by the following formula

$$P_{N+1}^{(n)}(x) = x P_N^{(n)}(x) + (N+n) P_N^{(n)}(x) \quad (39)$$

Assuming that the deflection function is in the form

$$\begin{aligned} u(x) &= \sum_{i=1}^N L_i(x) u_i \\ w(x) &= \sum_{i=1}^N L_i(x) w_i \end{aligned} \quad (40)$$

With  $L_i$  is the Lagrange polynomial, and  $u_i = u(x_i)$ ,  $w_i = w(x_i)$  are the displacements of the Gauss Lobatto quadrature points or the DQ nodal displacements of the beam finite element.

Using DQ rules and Gauss-Lobatto quadrature the expressions of kinetic energy and strain energy (41-42) can be written as follows

$$\begin{aligned} E_{ca} = \frac{1}{2} \left( \left( \dot{U}_0^T \sqrt{I_m} C \sqrt{I_m} \dot{U}_0 + \dot{V}_0^T \sqrt{I_m} C \sqrt{I_m} \dot{V}_0 + \dot{W}_0^T \sqrt{I_m} C \sqrt{I_m} \dot{W}_0 \right) + \left( \dot{\beta}_x^T \sqrt{I_d} C \sqrt{I_d} \dot{\beta}_x + \right. \right. \\ \left. \left. \dot{\beta}_y^T C \dot{\beta}_y \right) - 2\Omega \bar{\beta}_x^T \sqrt{I_p} C \sqrt{I_p} \dot{\beta}_y \right) \end{aligned} \quad (41)$$

With

$$I_m = 2\pi [C_1 \rho(r_1) r_1 \quad C_2 \rho(r_2) r_2 \quad \dots \quad C_N \rho(r_N) r_N] \quad (42)$$

$$I_d = \pi [C_1 \rho(r_1) r_1^3 \quad C_2 \rho(r_2) r_2^3 \quad \dots \quad C_N \rho(r_N) r_N^3] \quad (43)$$

$$I_p = 2\pi [C_1 \rho(r_1) r_1^3 \quad C_2 \rho(r_2) r_2^3 \quad \dots \quad C_N \rho(r_N) r_N^3] \quad (44)$$

$$\begin{aligned} E_{da} = \frac{1}{2} \bar{U}_0^T W^{(1)T} \sqrt{A_{11}} C \sqrt{A_{11}} W^{(1)} \bar{U}_0 + \frac{1}{2} \left[ \bar{\beta}_y^T W^{(1)T} \sqrt{B_{11}} C \sqrt{B_{11}} W^{(1)} \bar{\beta}_y + \right. \\ \left. \bar{\beta}_x^T W^{(1)T} \sqrt{B_{11}} C \sqrt{B_{11}} W^{(1)} \bar{\beta}_x \right] + \frac{1}{2} k_s \bar{\phi}^T W^{(1)T} \sqrt{B_{66}} C \sqrt{B_{66}} W^{(1)} \bar{\phi} + \\ \frac{1}{2} k_s \left[ \bar{V}_0^T W^{(1)T} \sqrt{(A_{55} + A_{66})} C \sqrt{(A_{55} + A_{66})} W^{(1)} \bar{V}_0 + \right. \\ \left. \bar{W}_0^T W^{(1)T} \sqrt{(A_{55} + A_{66})} C \sqrt{(A_{55} + A_{66})} W^{(1)} \bar{W}_0 + \right. \\ \left. \bar{\beta}_x^T \sqrt{(A_{55} + A_{66})} C \sqrt{(A_{55} + A_{66})} \bar{\beta}_x + \bar{\beta}_y^T \sqrt{(A_{55} + A_{66})} C \sqrt{(A_{55} + A_{66})} \bar{\beta}_y + \right. \\ \left. 2\bar{\beta}_x^T \sqrt{(A_{55} + A_{66})} C \sqrt{(A_{55} + A_{66})} W^{(1)} \bar{W}_0 - \bar{\beta}_y^T \sqrt{(A_{55} + A_{66})} C \sqrt{(A_{55} + A_{66})} W^{(1)} \bar{V}_0 \right] \end{aligned} \quad (45)$$

With  $W^{(1)}$  indicates the matrices of the weighting coefficients of the DQ rules for the first order derivatives respectively calculated with Eqs. (31)-(34), with respect to the Gauss-Lobatto nodes, and

$$C = \text{diag}[C_1 \quad C_2 \quad \dots \quad C_N] \quad (46)$$

Where  $C_j$  are the weighting coefficients of the Gauss-Lobatto integration.

$$\begin{cases} \bar{U}_0^T = [U_1 \ U_2 \ \dots \ U_N] \\ \bar{V}_0^T = [V_1 \ V_2 \ \dots \ V_N] \\ \bar{W}_0^T = [W_1 \ W_2 \ \dots \ W_N] \\ \bar{\Phi}^T = [\Phi_1 \ \Phi_2 \ \dots \ \Phi_N] \\ \bar{\beta}_y^T = [\beta_{y1} \ \beta_{y2} \ \dots \ \beta_{yN}] \\ \bar{\beta}_x^T = [\beta_{x1} \ \beta_{x2} \ \dots \ \beta_{xN}] \end{cases} \quad (47)$$

In order to construct an element that satisfies the requirements of continuity between elements, the element displacement vectors must be

$$u^T = [u_1 \ u'_1 \ u_3 \ \dots \ u_{N-2} \ u_N \ u'_N] \quad (48)$$

With  $u$  designates  $U_0, V_0, W_0, \Phi, \beta_y$  and  $\beta_x$

The relation between  $u$  and  $\bar{u}$  is defined using the DQ rule

$$u = Q\bar{u} \quad (49)$$

where

$$Q = \begin{bmatrix} 1 & 0 & 0 & \dots & 0 & 0 \\ W_{1,1}^{(1)} & W_{1,2}^{(1)} & W_{1,3}^{(1)} & \dots & W_{1,N-1}^{(1)} & W_{1,N}^{(1)} \\ 0 & 0 & 1 & \dots & 0 & 0 \\ \vdots & \vdots & \vdots & \ddots & \vdots & \vdots \\ 0 & 0 & 0 & \dots & 0 & 1 \\ W_{N,1}^{(1)} & W_{N,2}^{(1)} & W_{N,3}^{(1)} & \dots & W_{N,N-1}^{(1)} & W_{N,N}^{(1)} \end{bmatrix} \quad (50)$$

After replacing the displacements and rotations in the equations of kinetic and strain energies of the rotor system with the DQFEM weightings and applying the Lagrange's principle, it can deduce the elementary matrices of our system. The combination of these matrices yields the global matrices of the governing equation of motion of the rotor system, which are denoted as

$$[M]\{\ddot{q}\} + \Omega[G]\{\dot{q}\} + [K]\{q\} = \{0\} \quad (51)$$

[ $M$ ]. Mass matrix of the shaft.

[ $G$ ]. Gyroscopic matrix.

[ $K$ ]. Strain matrix.

Where

$$[M] = \begin{bmatrix} Q^{-T} \sqrt{I_m} C \sqrt{I_m} Q^{-1} & 0 & 0 & 0 & 0 & 0 \\ 0 & Q^{-T} \sqrt{I_m} C \sqrt{I_m} Q^{-1} & 0 & 0 & 0 & 0 \\ 0 & 0 & Q^{-T} \sqrt{I_m} C \sqrt{I_m} Q^{-1} & 0 & 0 & 0 \\ 0 & 0 & 0 & Q^{-T} \sqrt{I_p} C \sqrt{I_p} Q^{-1} & 0 & 0 \\ 0 & 0 & 0 & 0 & Q^{-T} \sqrt{I_d} C \sqrt{I_d} Q^{-1} & 0 \\ 0 & 0 & 0 & 0 & 0 & Q^{-T} \sqrt{I_d} C \sqrt{I_d} Q^{-1} \end{bmatrix} \quad (52)$$

$$[G] = \begin{bmatrix} 0 & 0 & 0 & 0 & 0 & 0 \\ 0 & 0 & 0 & 0 & 0 & 0 \\ 0 & 0 & 0 & 0 & 0 & 0 \\ 0 & 0 & 0 & 0 & 0 & 0 \\ 0 & 0 & 0 & 0 & 0 & \Omega I_p \sqrt{I_p} C \sqrt{I_p} \\ 0 & 0 & 0 & 0 & -\Omega I_p \sqrt{I_p} C \sqrt{I_p} & 0 \end{bmatrix} \quad (53)$$

$$[K] = \begin{bmatrix} [K_u] & 0 & 0 & 0 & 0 & 0 \\ 0 & [K_v] & 0 & 0 & 0 & [K_{v\beta_y}] \\ 0 & 0 & [K_w] & 0 & [K_{w\beta_x}] & 0 \\ 0 & 0 & 0 & [K_\emptyset] & 0 & 0 \\ 0 & 0 & [K_{\beta_x w}] & 0 & [K_{\beta_x}] & 0 \\ 0 & [K_{\beta_y v}] & 0 & 0 & 0 & [K_{\beta_y}] \end{bmatrix} \quad (54)$$

$$\left\{ \begin{array}{l} [K_u] = W^{(1)T} \sqrt{A_{11}} C \sqrt{A_{11}} W^{(1)} \\ [K_v] = k_s W^{(1)T} \sqrt{(A_{55} + A_{66})} C \sqrt{(A_{55} + A_{66})} W^{(1)} \\ [K_w] = k_s W^{(1)T} \sqrt{(A_{55} + A_{66})} C \sqrt{(A_{55} + A_{66})} W^{(1)} \\ [K_\emptyset] = k_s W^{(1)T} \sqrt{B_{66}} C \sqrt{B_{66}} W^{(1)} \\ [K_{\beta_x}] = W^{(1)T} \sqrt{B_{11}} C \sqrt{B_{11}} W^{(1)} + k_s \sqrt{(A_{55} + A_{66})} C \sqrt{(A_{55} + A_{66})} \\ [K_{\beta_y}] = W^{(1)T} \sqrt{B_{11}} C \sqrt{B_{11}} W^{(1)} + k_s \sqrt{(A_{55} + A_{66})} C \sqrt{(A_{55} + A_{66})} \\ [K_{v\beta_y}] = -k_s \sqrt{(A_{55} + A_{66})} C \sqrt{(A_{55} + A_{66})} W^{(1)} \\ [K_{w\beta_x}] = k_s \sqrt{(A_{55} + A_{66})} C \sqrt{(A_{55} + A_{66})} W^{(1)} \\ [K_{\beta_x w}] = [K_{w\beta_x}]^T \\ [K_{\beta_y v}] = [K_{v\beta_y}]^T \end{array} \right. \quad (55)$$

The assembly of the elementary matrices to obtain the total matrices is similar to that of the classical finite element method.

## 5. Validation

Efforts have been made to carefully validate this work with literature. Due to the scarcity as soon as important research work on the use of the FG shaft is available. Validation at each stage has been significantly confirmed by the literature.

Validation with the literature is carried out in order to determine the accuracy with which the grading of the material is carried out. The algorithm performed with the MATLAB programming language concerns different cases of gradation of the properties of the FG material. The material properties are calculated at the mean radius of each layer for different material laws, and its variation with the power law coefficient is graphically represented.

### 5.1 The variation of FG material properties in radial direction

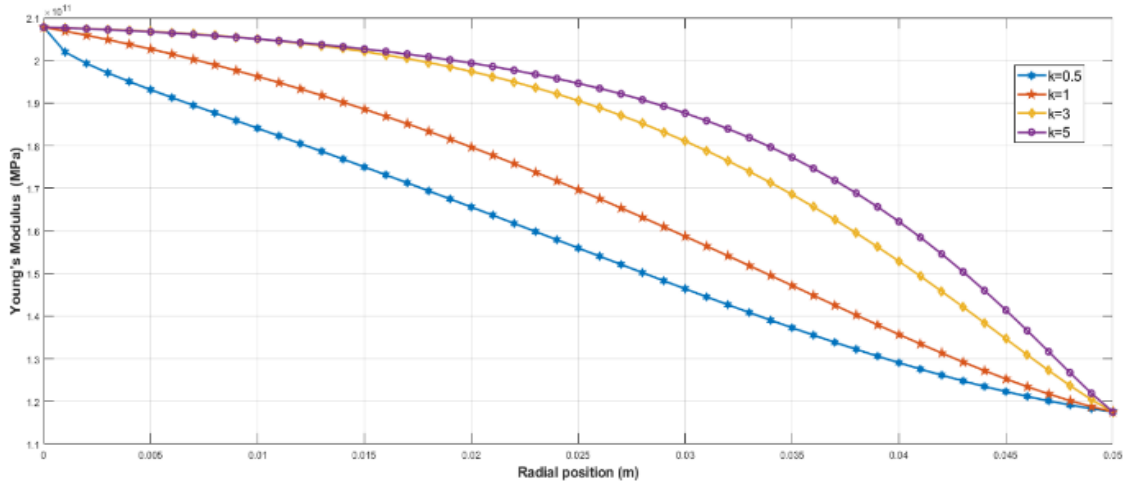


Fig. 11 Young's Modulus variation for different  $k$  values when  $T_m=300K$  and  $T_c= 900K$  for SS-ZrO2 FG shaft

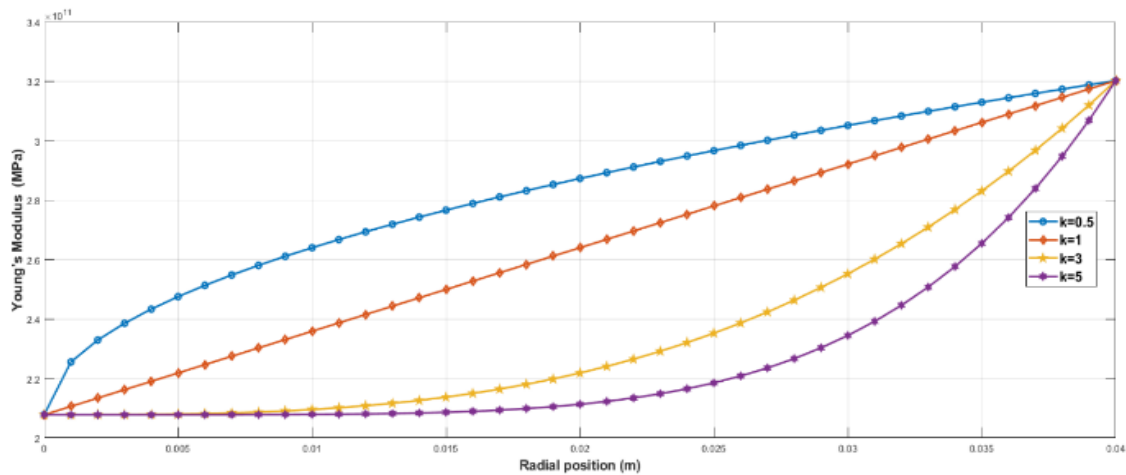


Fig. 12 Young's Modulus variation along the radial direction for different  $k$  values when for Al2O3 FG shaft at room temperature

The gradation of materials as a function of temperature, an FG shaft consisting of SS-ZrO2 was considered based on material data available in the literature (Reddy and Chin 1998). The radius ( $R_o$ ) of the shaft is taken as 50 mm, and the outer ceramic layer is kept at a temperature of 900K while the inner metal core is at room temperature 300K. The variation in material properties such as Young's modulus, Poisson's ratio and temperature the distribution profile has been showed in with Fig. 11 in the work of (Gayen *et al.* 2017b). The Young's modulus plot for different power laws, the coefficients obtained using the code are shown in Fig. 11. The algorithm was then applied to generate a material distribution profile for a 40 mm outer radius FG shaft made of SS-Al2O3, where the outer ceramic surface and the metal of the inner core were maintained at room temperature. Fig. 12. Shows that the resulting radial material variations are in good agreement with the patterns obtained from the literature work (Gayen *et al.* 2018).

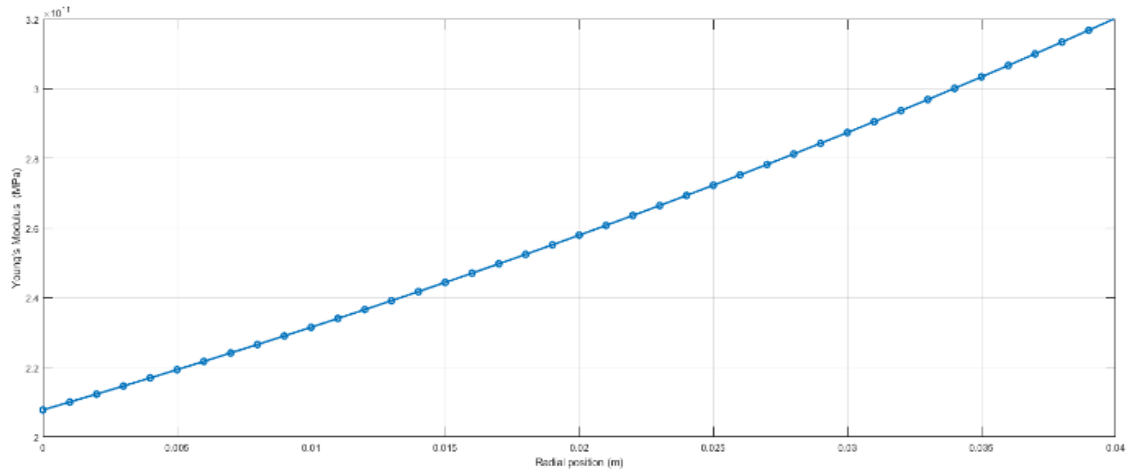


Fig. 13 Young's Modulus variation along the radial direction using exponential law for SS-Al2O3 FG shaft at room temperature

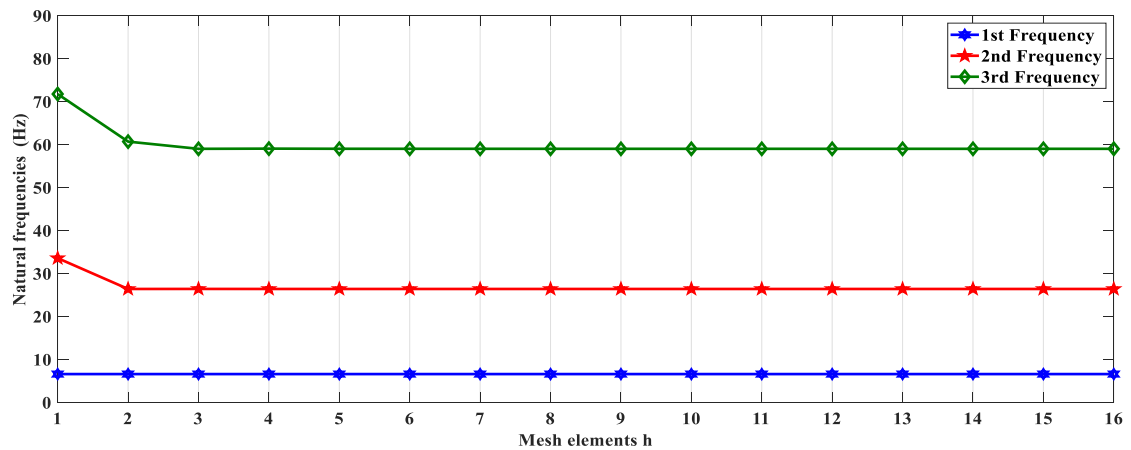


Fig. 14 Convergence of natural frequency with respect to the mesh element h and a sampling point equal to  $N=5$

### 5.2 Study of convergence.

To do the convergence of the modelling method we vary the sampling points number  $N$  and the mesh elements number  $h$  to see the speed of the convergence. A shaft with inner material is SUS304 and the outer material is Nickel (Ni), the mechanical properties of these two poles are shown in Tables 1 and 2 respectively. Geometrical dimensions (layer thickness FG  $h=0.002$  m, ratio diameter thickness  $D_L/h = 500$ , ratio length diameter  $L/D_L = 20$ , and a shear correction factor  $K_s=0.5$ . The outside and inside temperature is 300K.

Figs. 14-16 showing the convergence of the four Eigen frequencies with respect to the sampling number  $N$  and the number of mesh elements  $h$ , of a rotating FG shaft composed of Nickel (Ni) and SUS304 stainless steel, with boundary conditions simply supported in both ends. The figures show

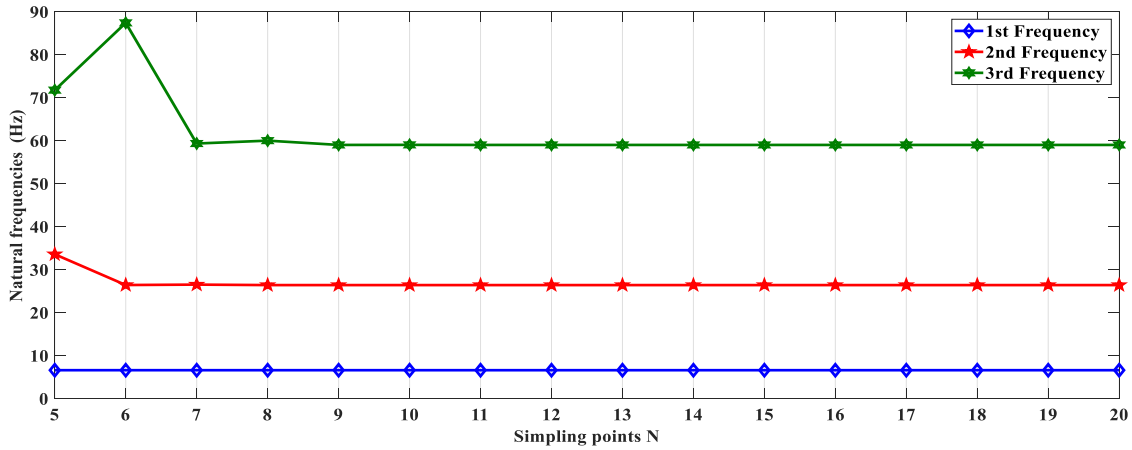


Fig. 15 Convergence of natural frequency with respect to the sampling point N and one mesh element h=1

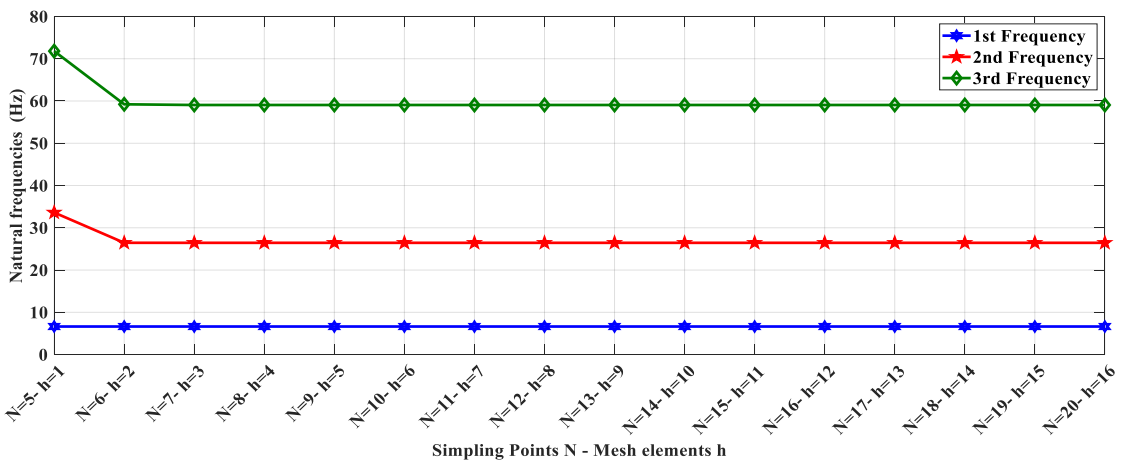


Fig. 16 Convergence of natural frequency with respect to the sampling point N and mesh element h

that the first three natural frequencies converge rapidly. We can see that the first frequency start converging at  $N=7$  in Fig. 15, and  $h=3$  in Fig. 14. However, in the combination between  $N$  and  $h$  it starts converging at  $N=6, h=2$ . The second frequency start converging at  $N=10$  in Fig. 15, and  $h=7$  in Fig. 14. However, in the combination between  $N$  and  $h$  it starts converging at  $N=7, h=3$ . It concluded that the combination between the two methods DQM and FEM gives good convergence with small sampling numbers  $N$  and mesh numbers  $h$ , which makes the method acceptable.

For more details of Figs. 14-16, see Table 2.

Therefore, in subsequent calculations,  $N=7$  and  $h=3$  is used.

### 5.3 Validation with a cylindrical FG shaft

To do the validation with a cylindrical shaft FG it is sufficient to put the angle of inclination in Eq. (29),  $\alpha=0$ . The same shaft as in (Loy *et al.* 1999) has been used, such that the inner material is SUS304 and the outer material is Nickel (Ni), the mechanical properties of these two poles are

Table 2 Convergence of natural frequency with rotational speed  $\Omega=0$ 

N	$f_1$	$f_2$	$f_3$	h	$f_1$	$f_2$	$f_3$	N-h	$f_1$	$f_2$	$f_3$
5	6.6413	33.6134	71.8006	1	6.6413	33.6134	71.8006	5-1	6.6413	33.6134	71.8006
6	6.6435	26.4607	87.4568	2	6.6420	26.4441	60.7320	6-2	6.6415	26.4526	59.2184
7	6.6415	26.5566	59.3804	3	6.6415	26.4545	59.0531	7-3	6.6415	26.4448	59.0544
8	6.6415	26.4448	60.0532	4	6.6415	26.4466	59.0969	8-4	6.6415	26.4448	59.0544
9	6.6415	26.4453	59.0572	5	6.6415	26.4453	59.0662	9-5	6.6415	26.4448	59.0544
10	6.6415	26.4448	59.0688	6	6.6415	26.4449	59.0585	10-6	6.6415	26.4448	59.0544
11	6.6415	26.4448	59.0544	7	6.6415	26.4448	59.0561	11-7	6.6415	26.4448	59.0544
12	6.6415	26.4448	59.0545	8	6.6415	26.4448	59.0552	12-8	6.6415	26.4448	59.0544
13	6.6415	26.4448	59.0544	9	6.6415	26.4448	59.0548	13-9	6.6415	26.4448	59.0544
14	6.6415	26.4448	59.0544	10	6.6415	26.4448	59.0546	14-10	6.6415	26.4448	59.0544
15	6.6415	26.4448	59.0544	11	6.6415	26.4448	59.0545	15-11	6.6415	26.4448	59.0544
16	6.6415	26.4448	59.0544	12	6.6415	26.4448	59.0545	16-12	6.6415	26.4448	59.0544
17	6.6415	26.4448	59.0544	13	6.6415	26.4448	59.0545	17-13	6.6415	26.4448	59.0544
18	6.6415	26.4448	59.0544	14	6.6415	26.4448	59.0544	18-14	6.6415	26.4448	59.0544
19	6.6415	26.4448	59.0544	15	6.6415	26.4448	59.0544	19-15	6.6415	26.4448	59.0544
20	6.6415	26.4448	59.0544	16	6.6415	26.4448	59.0544	20-16	6.6415	26.4448	59.0544

Table 3 Variation in natural vibration frequencies as a function of the power law index with rotation speed  $\Omega=0$ 

Material gradation	POWER LAW				EXP LAW		
	DQM	DQFEM	$h$ - $p$ FEM (Assem <i>et al.</i> 2022)	(Loy <i>et al.</i> 1999)		DQM	DQFEM
0	13.3459	13.2355	13.2537	12.894	100% Ni	13.1524	13.2355
0.5	13.5626	13.4502	13.4667	13.103			
0.7	13.6149	13.5022	13.5181	13.154			
1	13.6743	13.5611	13.5766	13.211	EXP FG		
2	13.7883	13.6742	13.6889	13.321	(Ni-SUS304)	13.4801	13.5652
5	13.9048	13.7897	13.8036	13.433			
15	13.9789	13.8631	13.8766	13.505			
30	14.0005	13.8848	13.8980	13.526	100% SUS304	13.8204	13.9077

shown in Tables 1 and 2 respectively. And geometrical dimensions (layer thickness FG  $h=0.002$  m, ratio diameter thickness  $D_L/h = 1000$ , ratio length diameter  $L/D_L = 10$ , and a shear correction factor  $K_s=0.5$ . The outside and inside temperature is 300K.

Prior to validation with the literature a convergence study of the results of the same shaft was made with the  $h$ - $p$  version of the finite element method and the DQM, see Figs. 10-11.

Table 3 shows the results of the validation with that found in (Assem *et al.* 2022) and (Loy *et al.* 1999), it can be seen that the difference in results between the methods is small.

Table 4 represents the validation of the natural frequencies of this method with the work in the literature, such that the geometric and physical parameters of the shaft are as follows: The diameter  $D$  and the total length  $L$  of the solid shaft are respectively 0.05 m and 0.9 m. The modulus of elasticity  $E$ , the density  $\rho$  and the Poisson's ratio  $\nu$  are

$$E=2 \times 10^{11} \text{ N/m}^2, \nu=0.3, \rho=7800 \text{ kg/m}^3.$$

Table 4 Natural vibration frequencies of isotropic rotating shaft with rotation speed  $\Omega = 10^4$

Rotating speed $\Omega$ [rad/s]	$\Omega = 10^4$							
	Backward mode (B)				Forward mode (F)			
Bending mode $\omega$ [Hz]	Present	(Boukhalfa 2014)	(René-Jean 1988)	(Assem <i>et al.</i> 2022)	Present	(Boukhalfa 2014)	(René-Jean 1988)	<i>h-p</i> FEM (Assem <i>et al.</i> 2022)
1	122.2145	122.3467	119.7548	122.3144	122.7438	134.2918	125.8150	122.9479
2	487.6529	484.6529	479.0191	487.8729	490.2952	530.4377	503.2598	490.3922
3	1092.4635	1073.5822	1077.7931	1092.5785	1098.0896	1169.8098	1132.3346	1098.1938

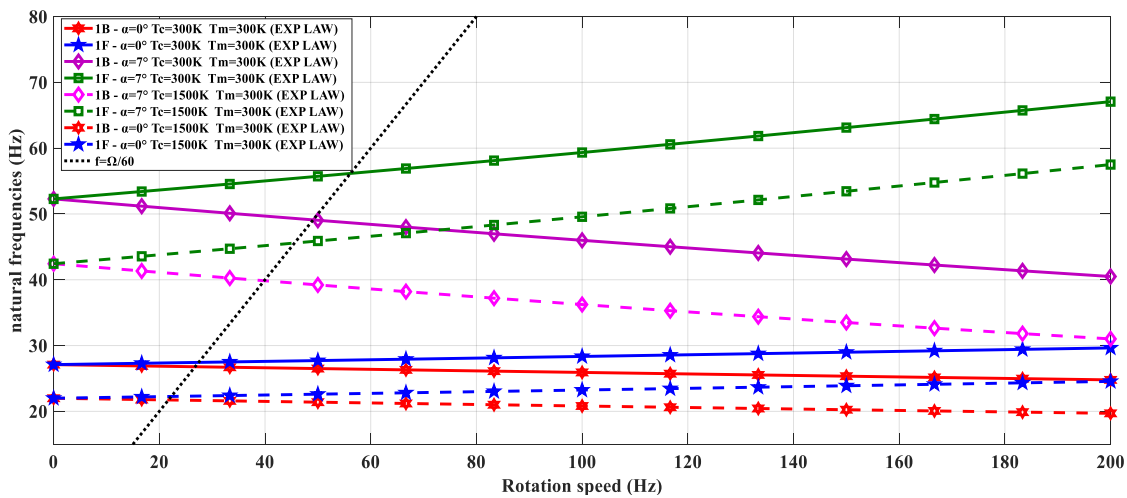


Fig. 17 Campbell's diagram of the bending of the first mode of the tapered FG rotor shaft simply supported ((F) forward modes (B) backward modes)-exponential law

### 6. Influence of the conical angle $\alpha$ of the hollow FG tapered shaft.

In this section, the influence of the cone angle  $\alpha$  on the natural frequencies of a hollow FG tapered shaft with simple supports at both ends is studied. The geometrical system dimensions (FG layer thickness  $h=0.002$  m, diameter to thickness ratio  $D_L / h = 500$ ), and a shear correction factor  $K_s=0.5$ . The cone angle ( $\alpha$ ) varies between  $0^\circ$  and  $7^\circ$ , because usually the cone angle of a rotor shaft rarely exceeds  $7^\circ$ . With a slenderness ratio set at  $L/D_L=10$ .

The tapered shaft FG consists of Nickel (Ni) as outer material and stainless steel (SUS304) as inner material. The external and internal temperature is 300K in one case, and the external and internal temperature is 1500K, 300K respectively in the second case.

Figs. 17-18 shows the Campbell diagram for two different conical angles ( $\alpha=0^\circ$  and  $\alpha=7^\circ$ ), for an FG tapered shaft made of Ni-SUS304. The results in Fig. 17 are obtained with the exponential distribution of FG, and the results in Fig. 18 are obtained with the power distribution with an index of volume fraction equal to 0.5.

According to the results presented in Tables 5-6, with a rotation speed equal to 10 Hz it can be seen that the results calculated with the Exponential Law are close to the results calculated with the Power Law with a volume index fraction equal to 1 in an ambient temperature of 300K.

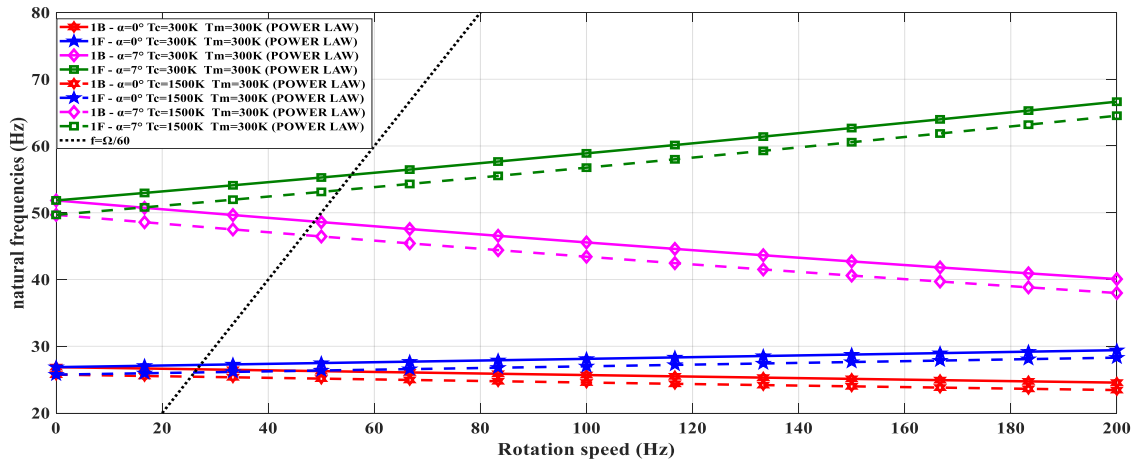


Fig. 18 Campbell's diagram of the bending of the first mode of the tapered FG rotor shaft simply supported ((F) forward modes (B) reverse modes)-power law  $k=0.5$

Table 5 Variation of natural frequencies as a function of the cone angle  $\alpha$  (outer Ni- inner SUS304)

Internal temperature=300K/External temperature=300K							
$\alpha^\circ$	POWER LAW						EXP-LAW
	$k=0.5$	$k=0.7$	$k=1$	$k=3$	$k=5$	$k=10$	
0°	26.8738	26.9774	27.0952	27.4359	27.5520	27.6586	27.1034
1°	31.2655	31.3861	31.5231	31.9195	32.0545	32.1785	31.5326
2°	35.2649	35.4009	35.5555	36.0026	36.1548	36.2947	35.5662
3°	38.9753	39.1257	39.2965	39.7906	39.9589	40.1134	39.3084
4°	42.4563	42.6201	42.8062	43.3444	43.5277	43.6960	42.8191
5°	45.7455	45.9221	46.1226	46.7025	46.8999	47.0813	46.1365
6°	48.8685	49.0571	49.2713	49.8908	50.1018	50.2955	49.2862
7°	51.8436	52.0437	52.2709	52.9281	53.1519	53.3574	52.2867
8°	54.6841	54.8952	55.1349	55.8281	56.0641	56.2809	55.1515
9°	57.4006	57.6221	57.8737	58.6014	58.8491	59.0766	57.8912
10°	60.0010	60.2326	60.4956	61.2563	61.5152	61.7530	60.5139

However, it changes widely when the gap is large between the internal and external temperature.

It can also be seen that as the conical angle increases, the frequencies increase. On the other hand, the influence of temperature causes the frequencies to decrease.

It is noted from the results presented in Tables 5-6 that the frequencies increase with the increase of the conical angle  $\alpha$ , whatever the deference between the external and internal temperature, which is physically explained that the system becomes more resistant to vibration responses. The results in Table 6 show that the increase in conical angle compensates for the decrease in frequencies due to temperature increases, making the rotor movement more resistant to vibration responses.

It can be seen from Tables 5-6 that the frequencies increase with respect to the increase in the fraction volume index, which is logical, since at  $k=0$  the FG layer is 100% external metal which is the Nickel, and nickel has greater thermal conductivity compared to that of the SUS304 metal.

Table 6 Variation of natural frequencies as a function of the cone angle  $\alpha$  (outer Ni-inner SUS304)

Internal temperature=300K/External temperature=300K							
$\alpha^\circ$	POWER LAW						EXP-LAW
	$k=0.5$	$k=0.7$	$k=1$	$k=3$	$k=5$	$k=10$	
0°	25.7530	26.0672	26.3854	27.1511	27.3750	27.5800	21.9929
1°	29.9622	30.3277	30.6978	31.5884	31.8488	32.0871	25.5884
2°	33.7955	34.2076	34.6250	35.6294	35.9229	36.1917	28.8627
3°	37.3518	37.8073	38.2685	39.3783	39.7027	39.9997	31.9004
4°	40.6882	41.1843	41.6867	42.8954	43.2488	43.5721	34.7503
5°	43.8407	44.3752	44.9165	46.2188	46.5994	46.9478	37.4432
6°	46.8340	47.4050	47.9832	49.3742	49.7808	50.1530	40.0000
7°	49.6854	50.2911	50.9045	52.3802	52.8115	53.2062	42.4357
8°	52.4080	53.0468	53.6938	55.2502	55.7051	56.1214	44.7612
9°	55.0116	55.6821	56.3612	57.9948	58.4723	58.9093	46.9852
10°	57.5040	58.2049	58.9148	60.6223	61.1214	61.5781	49.1142

Table 7 Variation of natural frequencies as a function of the cone angle  $\alpha$  (outer Al2O3-inner SUS304)

Internal temperature=300K/External temperature=300K							
$\alpha^\circ$	POWER LAW						EXP-LAW
	$k=0.5$	$k=0.7$	$k=1$	$k=3$	$k=5$	$k=10$	
0°	40.0427	38.2487	36.3785	31.7361	30.3567	29.1604	36.8773
1°	46.5846	44.4974	42.3214	36.9207	35.3163	33.9250	42.9017
2°	52.5422	50.1878	47.7334	41.6422	39.8329	38.2639	48.3879
3°	58.0693	55.4671	52.7545	46.0226	44.0231	42.2894	53.4778
4°	63.2546	60.4200	57.4650	50.1321	47.9543	46.0659	58.2529
5°	68.1543	65.1000	61.9160	54.0153	51.6688	49.6344	62.7649
6°	72.8064	69.5435	66.1421	57.7022	55.1957	53.0226	67.0490
7°	77.2380	73.7764	70.1680	61.2144	58.5554	56.2502	71.1300
8°	81.4694	77.8180	74.0119	64.5678	61.7633	59.3319	75.0266
9°	85.5158	81.6830	77.6878	67.7747	64.8310	62.2790	78.7529
10°	89.3895	85.3830	81.2068	70.8447	67.7677	65.1002	82.3201

Table 8 Variation of natural frequencies as a function of the cone angle  $\alpha$  (outer Al2O3-inner SUS304)

Internal temperature=300K/External temperature=1500K							
$\alpha^\circ$	POWER LAW						EXP-LAW
	$k=0.5$	$k=0.7$	$k=1$	$k=3$	$k=5$	$k=10$	
0°	39.2519	37.6080	35.8802	31.5383	30.2364	29.0950	30.3795
1°	45.6651	43.7523	41.7420	36.6908	35.1764	33.8490	35.3435
2°	51.5054	49.3478	47.0802	41.3831	39.6752	38.1782	39.8642
3°	56.9238	54.5390	52.0327	45.7363	43.8489	42.1948	44.0582
4°	62.0070	59.4091	56.6790	49.8203	47.7646	45.9629	47.9928
5°	66.8103	64.0110	61.0693	53.6794	51.4645	49.5234	51.7107
6°	71.3708	68.3804	65.2377	57.3434	54.9774	52.9040	55.2407
7°	75.7152	72.5427	69.2087	60.8339	58.3239	56.1244	58.6034
8°	79.8632	76.5168	73.0001	64.1665	61.5192	59.1993	61.8141
9°	83.8300	80.3173	76.6258	67.3535	64.5748	62.1398	64.8846
10°	87.6275	83.9555	80.0968	70.4045	67.4999	64.9547	67.8239

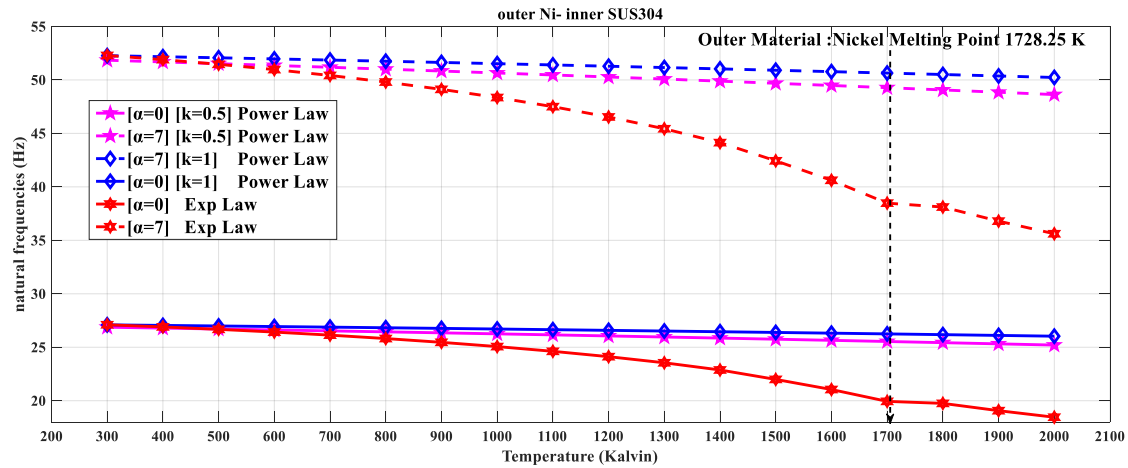


Fig. 19 Temperature-dependent variation of the first frequency, (outer Ni-inner SUS304)

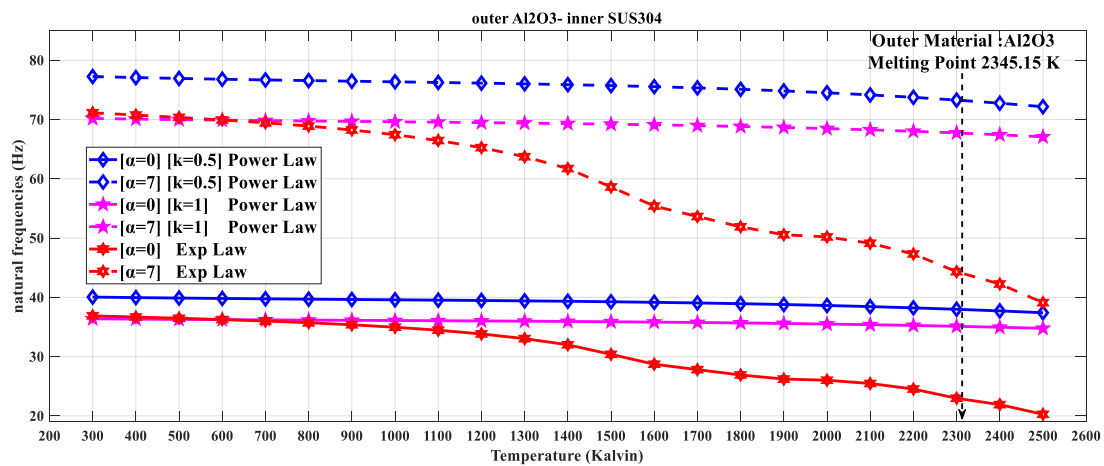


Fig. 20 Temperature-dependent variation of the first frequency, (outer Al<sub>2</sub>O<sub>3</sub>-inner SUS304)

On the other hand, in Tables 7-8, we notice the reverse, which is the decrease in frequencies compared to the increase in the fraction volume index, because the external metal is Al<sub>2</sub>O<sub>3</sub>, which has a lower conductivity. Thermal compared to SUS304.

## 7. Influence of external temperature on natural frequencies.

In this section, the shaft studied is the same as the one in the previous section, only the temperature and the composition of FG materials are changed.

The external temperature is varied from 300K to 1500K, keeping the internal metal temperature fixed at 300K.

Figs. 19-22 depict the frequencies of four different types of FG mixes (AL<sub>2</sub>O<sub>3</sub>-SUS304, Ni-SUS304, Silicone nitrid-SUS304, Zirconia-SUS304). The silicon nitrid-SUS304 and AL<sub>2</sub>O<sub>3</sub>-

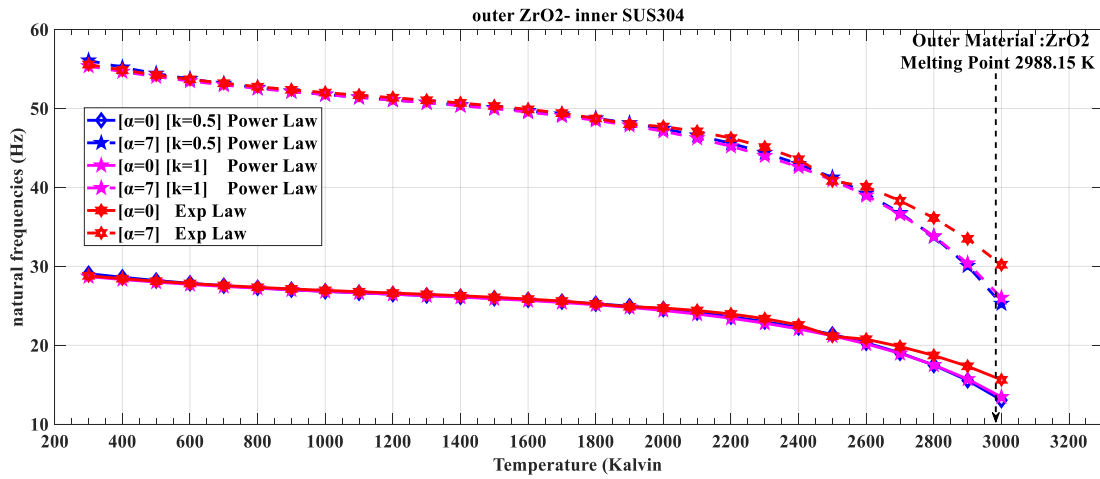


Fig. 21 Temperature-dependent variation of the first frequency, (outer Zirconia-inner SUS304)

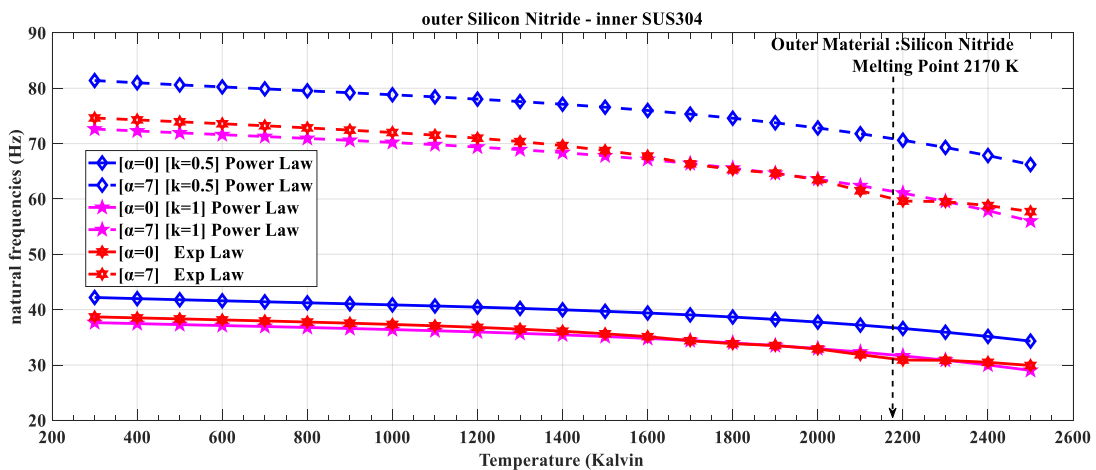


Fig. 11 Temperature-dependent variation of the first frequency, (outer Silicon Nitride-inner SUS304)

SUS304 mixtures have the highest frequencies in all cases, according to these results (Figs. 19-22). It explains why silicone nitrid-SUS304 and AL2O3-SUS304 mixtures outperform other mixtures in terms of temperature resistance. The frequencies of the mixtures Ni-SUS304, Zr-SUS304, are very close.

Note that as the cone angle increases, the more vibration-resistant the deflecting system becomes (i.e., the natural frequencies increase). On the other hand, the influence of temperature always decreases the frequencies and makes the system less resistant to vibration. The FG material distribution method has a great influence on the dynamic and thermal behaviour of the FG shaft. For all of the FG materials tested in this study, the frequencies fall as the temperature rises, albeit in varied quantities. As a result, each FG material has a different temperature resistance. It is clear that as the temperature rises, the FG shaft becomes increasingly unstable.

In this section, three cases of FGM law are shown, in case for the power law for a fraction volume index equal to 0.5 and 1, and also the exponential law. We notice between the results

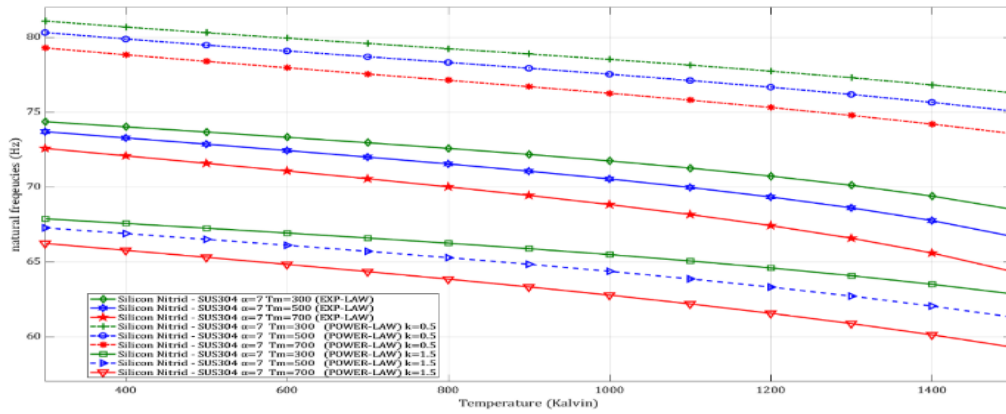


Fig. 23 Variation of the 1st frequency under the interne and external thermal gradient for a conical angle equal to  $7^\circ$

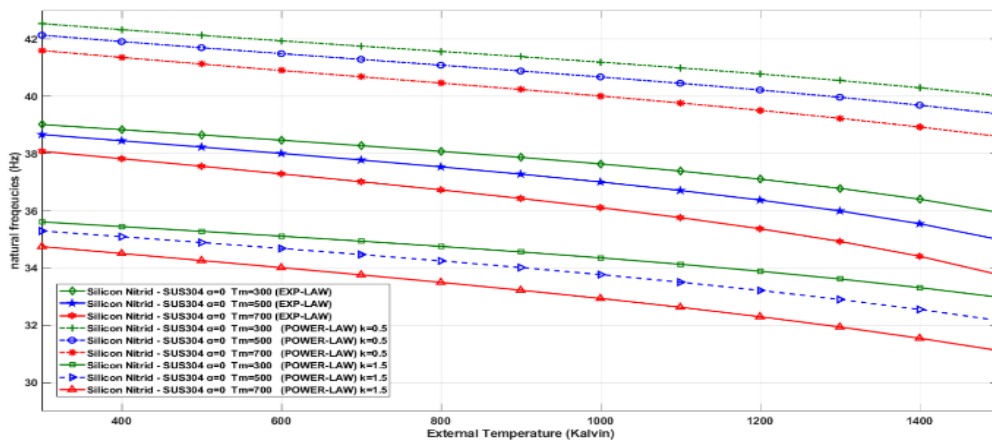


Fig. 24 Variation of the 1st frequency under the interne and external thermal gradient for a conical angle equal to  $0^\circ$

calculate with the fraction volume index which is equal to 0.5 and the fraction volume index which is equal to 1, that the interval of decreasing frequencies relative to increasing temperature, increase with increasing fraction volume index. Because in the power law, the greater the fraction volume index, the thinner the outer ceramic layer, that is, the less resistance to temperature change.

### 7.1 Internal temperature influence

In this section the external temperature (ceramic temperature) is varied for deferent internal temperature (metal temperature  $T_m$ ), and a combination between Silicon Nitride and SUS304 stainless steel. The frequencies in this section are obtained with a rotation speed equal to 0 rpm.

According to Figs. 23 and 24, the difference between the frequency curves decreases with the increase in the internal temperature of the metal  $T_m$  in the case of graduation with the power law. On the other hand, with the exponential gradation, the difference between the frequencies curves increases with the increase in internal temperature.

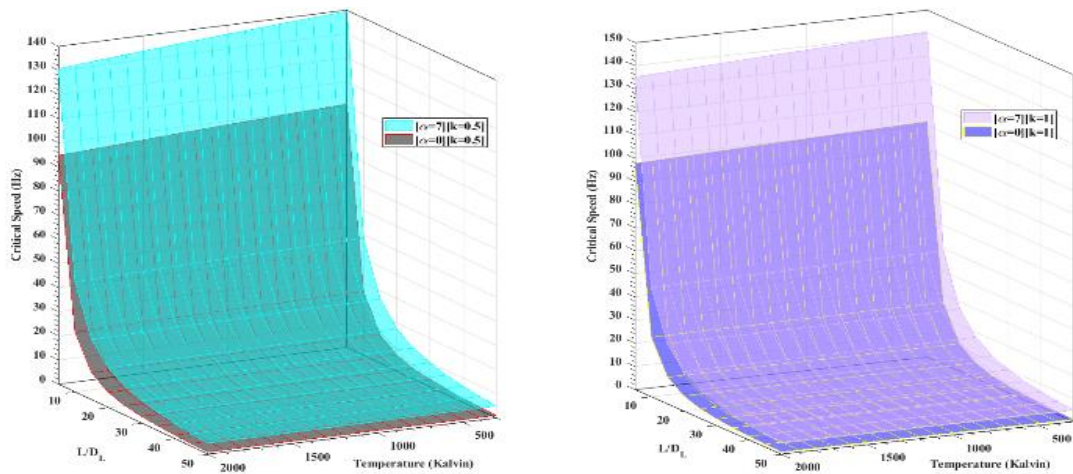


Fig. 25 Temperature-dependent variation of the first critical speed, (outer Ni-inner SUS304)

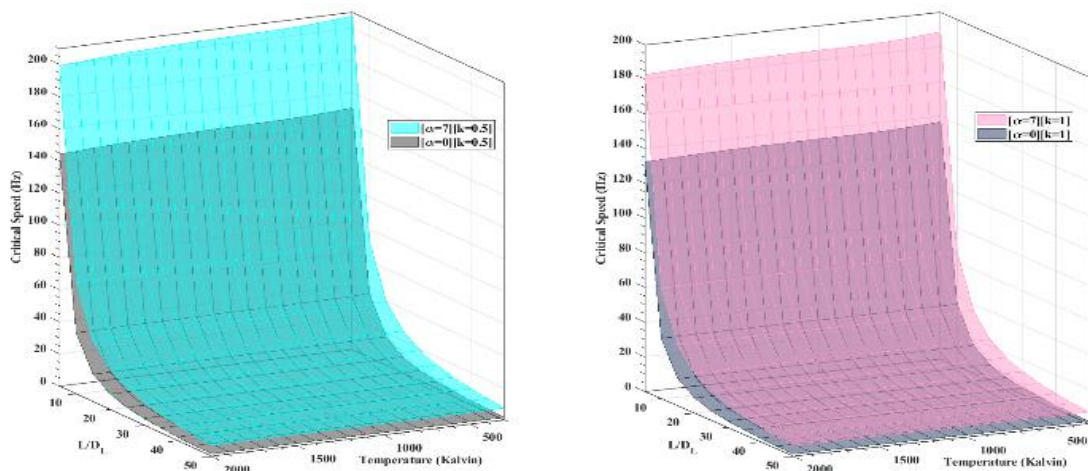


Fig. 26 Temperature-dependent variation of the first critical speed, (outer Al<sub>2</sub>O<sub>3</sub>-inner SUS304)

## 8. Influence of external temperature and length-diameter ratio on natural frequencies

Figs. 25-26 illustrate the influence of Temperature and length-diameter ratio with two conicity angles  $\alpha = [0, 7]$  and a power law index  $k = [0.5, 1]$ , on the behaviour of critical speed of the rotating tapered shaft. It is noticed that the critical velocities have the same behaviour as the natural frequencies. On the other hand, it can be seen that the increase in value of temperature reduces the critical speeds of the rotor, which is physically logical because the shaft loses its rigidity by increasing the temperature. In addition, the increase in the length-to-diameter ratio, the critical speeds decrease, and this is due to the low resistance to bending when the length-to-diameter ratio is high. The most important effect in this study is that the rise of conicity angle increases the value of critical speeds, whatever the value of the temperature, which explains that the more the conicity angle increases, the rotor becomes more resistant to bending critical speeds.

## 9. Conclusions

In this paper, the differential quadrature method combined with Timoshenko's beam theory, taking into account the gyroscopic effect and the rotational inertia was performed to study the vibration characteristics of FG tapered rotating shafts simply supported on a ceramic base. Several FG mixtures were used. The elements of the FG tapered shaft are modelled with two different gradations, the gradation of the power law with NLTD and the exponential gradient with ETD. Several examples have been processed to determine the effect of the cone angle ( $\alpha$ ) and the influence of temperature on the fundamental frequencies of the FG tapered rotor shafts. The following conclusions can be drawn from this work:

- The differential quadrature method shows good convergence and results close to those found in the literature.
- The taper of the shaft makes the system more resistant to vibrations, which explains why the frequencies increasing with the increase of the conical angle.
- In the case of the results obtained with the power law, the variation of the volume fraction index influences the frequency behaviour is noticed. By increasing the value of the volume fraction index, the frequencies approach the frequencies when the shaft is composed of 100% internal materials (metal), and it is also the same in the opposite direction, the more the volume fraction index is decreased, the more the frequencies approach the frequencies when the shaft is composed of 100% external materials (ceramic).
- The frequencies obtained with exponential gradation are close to those obtained with power law gradation with a fraction volume index equal to  $k=1$ .
- The results show that the frequencies decrease with the increase in the external temperature gradient, regardless of the type of ceramic, but with different proportions, which explains the temperature resistance difference of each ceramic. In the ceramic examples treated in this paper, Silicon Nitride is the most temperature resistant; Aluminium Oxide ( $Al_2O_3$ ) comes second.
- The advantage of using an FG shaft instead of a homogeneous shaft is the resistance to temperature effects on frequency behaviour; this is clearly inferred from the results.
- The advantage of the taper angle in the geometry of the FG shaft is that it considerably increases the resistance of the FG shaft, which in the result explains the increase in frequencies.
- By increasing the temperature, the drop in the natural frequencies of the FG shaft is more stable than that of a homogeneous shaft in SUS304.
- The influence of temperature causes the natural frequencies to decrease; on the other hand, it has been found that the increase of the conical angle causes the natural frequencies to increase. Therefore, it was concluded that to avoid significant decreases in frequencies relative to temperature, the geometric parameter of conical angle is increased, and to make the structure of the shaft more resistant to the influence of temperature.
- A rotor shaft under the influence of temperature is exposed to hazardous frequencies and critical speeds due to the change in the material's mechanical characteristics due to temperature. The addition of FG materials gives significant resistance to temperature influence, which implies resistance to vibration frequencies. In this work, the geometric parameter of the conical angle was used, to optimize the resistance to the frequencies of vibrations.

## Acknowledgments

We acknowledge with grateful thanks the support by the laboratory of mechanical and material

systems engineering in university of Tlemcen, as well as the General Directorate of Scientific Research and Technological Development of the Ministry of Higher Education of Algeria.

## References

- Aboudi, J., Pindera, M.J. and Arnold, S.M. (1999), "Higher-order theory for functionally graded materials", *Compos. Part B: Eng.*, **30**(8), 777-832. [https://doi.org/10.1016/S1359-8368\(99\)00053-0](https://doi.org/10.1016/S1359-8368(99)00053-0).
- Afsar, A.M. and Go, J. (2010), "Finite element analysis of thermoelastic field in a rotating FGM circular disk", *Appl. Math. Model.*, **34**(11), 3309-3320. <https://doi.org/10.1016/j.apm.2010.02.022>.
- Afshari, H. and Irani Rahaghi, M. (2018), "Whirling analysis of multi-span multi-stepped rotating shafts", *J. Brazil. Soc. Mech. Sci. Eng.*, **40**(9), 424. <https://doi.org/10.1007/s40430-018-1351-x>.
- Afshari, H., Torabi, K. and Jafarzadeh Jazi, A. (2022), "Exact closed form solution for whirling analysis of Timoshenko rotors with multiple concentrated masses", *Mech. Bas. Des. Struct. Mach.*, **50**(3), 969-992. <https://doi.org/10.1080/15397734.2020.1737112>.
- Ahmed, S., Abdelhamid, H., Ismail, B. and Ahmed, F. (2020), "An differential quadrature finite element and the differential quadrature hierarchical finite element methods for the dynamics analysis of on board shaft", *Eur. J. Comput. Mech.*, **29**(4-6), 1. <https://doi.org/10.13052/ejcm1779-7179.29461>.
- Akbaş, Ş.D. (2014), "Free vibration of axially functionally graded beams in thermal environment", *Int. J. Eng. Appl. Sci.*, **6**(3), 37-51. <https://doi.org/10.24107/ijeas.251224>.
- Assem, H., Hadjoui, A. and Saimi, A. (2022), "Numerical analysis on the dynamics behavior of FGM rotor in thermal environment using h-p finite element method", *Mech. Bas. Des. Struct. Mach.*, **50**(11), 3925-3948. <https://doi.org/10.1080/15397734.2020.1824791>.
- Berthelot, J.M. (1996), *Composite Materials, Mechanical Behavior and Analysis of Structures*, Second Edition, Masson.
- Bose, A. and Sathujoda, P. (2020), "Effect of thermal gradient on vibration characteristics of a functionally graded shaft system", *Math. Model. Eng. Prob.*, **7**(2), 212-222. <https://doi.org/10.18280/mmep.070207>.
- Boukhalfa, A. (2014), "Dynamic analysis of a spinning functionally graded material shaft by the p-version of the finite element method", *Lat. Am. J. Solid. Struct.*, **11**(11), 2018-2038. <https://doi.org/10.1590/S1679-78252014001100007>.
- Boukhalfa, A. and Hadjoui, A. (2010), "Free vibration analysis of an embarked rotating composite shaft using the hp-version of the FEM", *Lat. Am. J. Solid. Struct.*, **7**(2), 105-141. <https://doi.org/10.1590/S1679-78252010000200002>.
- Bouzidi, I., Hadjoui, A. and Fellah, A. (2021), "Dynamic analysis of functionally graded rotor-blade system using the classical version of the finite element method", *Mech. Bas. Des. Struct. Mach.*, **49**(7), 1080-1108. <https://doi.org/10.1080/15397734.2019.1706558>.
- Cheng, J., Xu, H. and Yan, A. (2006), "Frequency analysis of a rotating cantilever beam using assumed mode method with coupling effect", *Mech. Bas. Des. Struct. Mach.*, **34**(1), 25-47. <https://doi.org/10.1080/15367730500501587>.
- Ding, J., Chu, L., Xin, L. and Dui, G. (2018), "Nonlinear vibration analysis of functionally graded beams considering the influences of the rotary inertia of the cross section and neutral surface position", *Mech. Bas. Des. Struct. Mach.*, **46**(2), 225-237. <https://doi.org/10.1080/15397734.2017.1329020>.
- Gayen, D., Chakraborty, D. and Tiwari, R. (2017a), "Finite element analysis for a functionally graded rotating shaft with multiple breathing cracks", *Int. J. Mech. Sci.*, **134**, 411-423. <https://doi.org/10.1016/j.ijmecsci.2017.10.027>.
- Gayen, D., Chakraborty, D. and Tiwari, R. (2017b), "Whirl frequencies and critical speeds of a rotor-bearing system with a cracked functionally graded shaft-Finite element analysis", *Eur. J. Mech.-A/Solid.*, **61**, 47-58. <https://doi.org/10.1016/j.euromechsol.2016.09.003>.
- Gayen, D., Chakraborty, D. and Tiwari, R. (2018), "Free vibration analysis of functionally graded shaft system with a surface crack", *J. Vib. Eng. Technol.*, **6**(6), 483-494. <https://doi.org/10.1007/s42417-018->

- 0065-9.
- Gayen, D. and Roy, T. (2014), "Finite element based vibration analysis of functionally graded spinning shaft system", *Proc. Inst. Mech. Eng., Part C: J. Mech. Eng. Sci.*, **228**(18), 3306-3321. <https://doi.org/10.1177/0954406214527923>.
- Gayen, D., Tiwari, R., & Chakraborty, D. (2021). "Thermo-mechanical analysis of a rotor-bearing system having a functionally graded shaft with transverse breathing cracks", *Proceedings of the 6th National Symposium on Rotor Dynamics*, Springer, Singapore.
- Gayen, D., Tiwari, R. and D.C. (2019), "Static and dynamic analyses of cracked functionally graded structural components: A review", *Compos. Part B: Engineering*, **173**, 106982. <https://doi.org/10.1016/j.compositesb.2019.106982>.
- Hirai, T. and Chen, L. (1999a), "Recent and prospective development of functionally graded materials in Japan", *Mater. Sci. Forum*, **308**, 509-514. <https://doi.org/10.4028/www.scientific.net/MSF.308-311.509>.
- Holt, J.B., Koizumi, M., Hirai, T., & Munir, Z.A. (1993), *Ceramic Transactions: Functionally Graded Materials*, Volume 34 (No. CONF-921128-), American Ceramic Society, Westerville, OH, USA.
- Hua, L. and Lam, K.Y. (1998), "Frequency characteristics of a thin rotating cylindrical shell using the generalized differential quadrature method", *Int. J. Mech. Sci.*, **40**(5), 443-459. [https://doi.org/10.1016/S0020-7403\(97\)00057-X](https://doi.org/10.1016/S0020-7403(97)00057-X).
- Irani Rahagi, M., Mohebbi, A. and Afshari, H. (2016), "Longitudinal-torsional and two plane transverse vibrations of a composite timoshenko rotor", *J. Solid Mech.*, **8**(2), 418-434.
- Kiani, Y. and Eslami, M.R. (2010), "Thermal buckling analysis of functionally graded material beams", *Int. J. Mech. Mater. Des.*, **6**(3), 229-238. <https://doi.org/10.1007/s10999-010-9132-4>.
- Librescu, L., Oh, S.Y. and Song, O. (2005), "Thin-walled beams made of functionally graded materials and operating in a high temperature environment: Vibration and stability", *J. Therm. Stress.*, **28**(6-7), 649-712. <https://doi.org/10.1080/01495730590934038>.
- Loy, C.T., Lam, K.Y. and Reddy, J.N. (1999), "Vibration of functionally graded cylindrical shells", *Int. J. Mech. Sci.*, **41**(3), 309-324. [https://doi.org/10.1016/S0020-7403\(98\)00054-X](https://doi.org/10.1016/S0020-7403(98)00054-X).
- Chang, M.Y., Chen, J.K., & Chang, C.Y. (2004), "A simple spinning laminated composite shaft model", *Int. J. Solid. Struct.*, **41**(3-4), 637-662. <https://doi.org/10.1016/j.ijsolstr.2003.09.043>.
- Pouretamad, A., Torabi, K. and Afshari, H. (2019a), "DQEM analysis of free transverse vibration of rotating non-uniform nanobeams in the presence of cracks based on the nonlocal Timoshenko beam theory", *SN Appl. Sci.*, **1**(9), 1092. <https://doi.org/10.1007/s42452-019-1130-z>.
- Pouretamad, A., Torabi, K. and Afshari, H. (2019b), "Free vibration analysis of a rotating non-uniform nanocantilever carrying arbitrary concentrated masses based on the nonlocal timoshenko beam using DQEM", *INAE Lett.*, **4**(1), 45-58. <https://doi.org/10.1007/s41403-019-00065-x>.
- Przybyłowicz, P.M. (2005), "Stability of actively controlled rotating shaft made of functionally graded material", *J. Theor. Appl. Mech.*, **43**(3), 609-630.
- Rao, D.K. and Roy, T. (2016), "Vibration analysis of functionally graded rotating shaft system", *Procedia Eng.*, **144**, 775-780. <https://doi.org/10.1016/j.proeng.2016.05.084>.
- Reddy, J.N. and Chin, C.D. (1998), "Thermomechanical analysis of functionally graded cylinders and plates", *J. Therm. Stress.*, **21**(6), 593-626. <https://doi.org/10.1080/01495739808956165>.
- René-Jean, G. (1988), *Vibrations des Structures*, Vol. 69, La Collection R&D d'EDF Chez EYROLLES.
- Saimi, A. and Hadjoui, A. (2016), "An engineering application of the h-p version of the finite elements method to the dynamics analysis of a symmetrical on-board rotor", *Eur. J. Comput. Mech.*, **25**(5), 388-416. <https://doi.org/10.1080/17797179.2016.1245597>.
- Torabi, K., Afshari, H. and Haji Aboutalebi, F. (2014), "A DQEM for transverse vibration analysis of multiple cracked non-uniform Timoshenko beams with general boundary conditions", *Comput. Math. Appl.*, **67**(3), 527-541. <https://doi.org/10.1016/j.camwa.2013.11.010>.
- Torabi, K., Afshari, H. and Najafi, H. (2017), "Whirling analysis of axial-loaded multi-step timoshenko rotor carrying concentrated masses", *J. Solid Mech.*, **9**(1), 138-156.
- Touloukian, Y.S. (1966), *Thermophysical Properties of High Temperature Solid Materials*, Thermophysical and Electronic Properties Information Analysis Center Lafayette.

<https://apps.dtic.mil/sti/pdfs/AD0649950.pdf>.

Uemura, S. (2003), "The activities of FGM on new application", *Mater. Sci. Forum*, **423-425**, 1-10. <https://doi.org/10.4028/www.scientific.net/MSF.423-425.1>.

Xing, Y. and Liu, B. (2009), "High-accuracy differential quadrature finite element method and its application to free vibrations of thin plate with curvilinear domain", *Int. J. Numer. Meth. Eng.*, **80**(13), 1718-1742. <https://doi.org/10.1002/nme.2685>.

Yamanouchi, M., Koizumi, M., Hirai, T. and Shiota, I. (1990), "Proceedings of the first international symposium on functionally gradient materials", Sendai, Japan.

Zahi, R., Refassi, K. and Habib, A. (2018), "Dynamic calculation of a tapered shaft rotor made of composite material", *Adv. Aircraft Spacecraft Sci.*, **5**(1), 51-71. <https://doi.org/10.12989/aas.2018.5.1.051>.

CC